UV-induced photochemistry of 1,3-benzoxazole, 2-isocyanophenol, and 2-cyanophenol isolated in low-temperature Ar matrixes

Igor Reva,*[a,b] A. J. Lopes Jesus,*[c] Cláudio M. Nunes,[a]

José P. L. Roque [a] and Rui Fausto [a]

[a] *University of Coimbra, CQC, Department of Chemistry, 3004-535 Coimbra, Portugal*

[b] *University of Coimbra, CIEPQPF, Department of Chemical Engineering, 3030-790 Coimbra, Portugal*

[c] *University of Coimbra, QC, Faculty of Pharmacy, 3004-295 Coimbra, Portugal*

* *Corresponding authors. E-mail addresses:* reva@qui.uc.pt and ajorge@ff.uc.pt

ABSTRACT

Monomers of 1,3-benzoxazole isolated in cryogenic argon matrix were characterized by infrared spectroscopy. Photochemistry of the matrix-isolated 1,3-benzoxazole, induced by excitation with frequency-tunable narrowband UV light, was investigated. Irradiation at 233 nm resulted in a nearly quantitative conversion of 1,3-benzoxazole into 2-isocyanophenol. The individual photochemical behaviour of the *in situ* produced 2-isocyanophenol was studied upon excitations at 290 nm, where 1,3-benzoxazole does not react. Photochemistry of isomeric matrix-isolated 2-cyanophenol was also studied. The photoreactions of 2-substituted (cyano- or isocyano-) phenols were found to have many similarities: (i) OH bond cleavage, yielding 2-substituted (cyano- or isocyano-) phenoxyl radical and H-atom, (ii) recombination of the detached H-atom, resulting in an oxo tautomer, (iii) decomposition leading to fulvenone, together with HCN and HNC. In another photoprocess, 2-cyanophenol undergoes [1,5] H-shift from the hydroxyl to cyano group yielding isomeric ketenimine. Analogous [1,5] H-shift from the hydroxyl to isocyano group must have occurred also in 2-isocyanophenol; however, the resulting nitrile ylide isomer is kinetically unstable and collapses to benzoxazole. All photoproducts were characterized by comparison of their observed infrared spectra with those computed at the B3LYP/6-311++G(d,p) level. Mechanistic analysis of the photochemistry occurring in the family of the title compounds is presented.

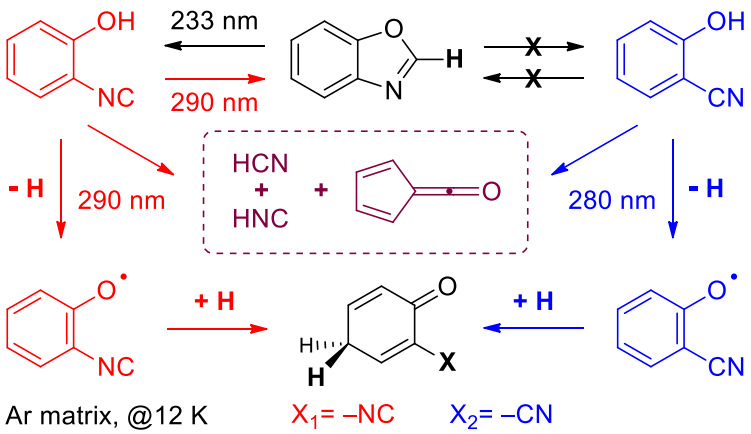

■ INTRODUCTION

1,3-Benzoxazole **1** (also known as benzo[*d*]oxazole, or benzoxazole) consists of an oxazole ring fused to a benzene ring (Scheme 1). It is the nucleus of numerous compounds with important biological, pharmacological and photophysical properties.[1-4] Its isomeric 1,2-benzisoxazole **2** (also known as benzo[*d*]isoxazole, or benzisoxazole) has isoxazole ring fused to a benzene ring (Scheme 1). They differ by the relative position of the oxygen and nitrogen atoms: in the oxazole, the two heteroatoms are separated by a carbon atom, while in the isoxazole they are bound directly. This key structural difference renders benzisoxazole to possess a weak N−O bond, making it much more reactive,[5-6] and consequently more prone to undergo chemical transformations than benzoxazole.

Scheme 1. Summary of the photo- and thermally induced reactivity of benzoxazole **1** and benzisoxazole **2** reported in literature.[7-12]

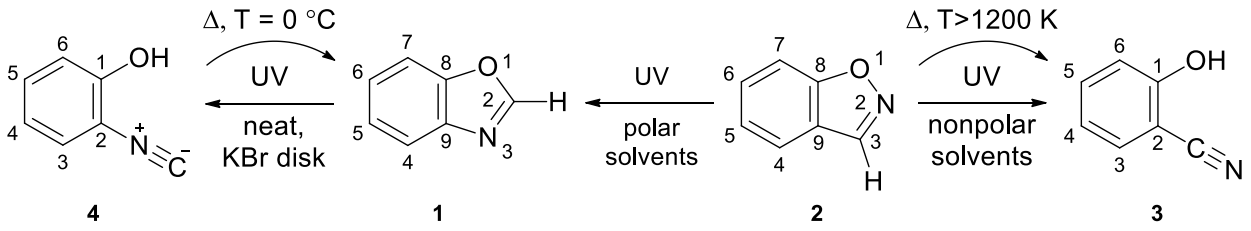

Interestingly, photoexcitation of 1,2-benzisoxazole **2** in polar solvents affords 1,3-benzoxazole **1**, whereas the photochemistry of **2** in non-polar solvents leads mainly to its open-ring isomer 2-cyanophenol **3** (Scheme 1).[7-11] The thermal reaction (single pulse shock-tube experiments, T>1200 K) of **2** results in its complete isomerization to **3** (Scheme 1), prior to fragmentation.[12] Data from luminescence measurements and from sensitization and quenching studies suggest that the lowest singlet excited state of benzisoxazole in non-polar solvents is an $^{l}(n,\pi)^*$ state, which undergoes intersystem crossing (ISC) to a triplet state, leading to **3**. On the contrary, in polar solvents the lowest singlet excited state of **2** is a $^{l}(\pi,\pi)^*$ state, which leads to faster conversion of the compound into **1** than ISC to the triplet manifold.[10] Nevertheless, the photochemistry of benzisoxazole is still puzzling. Low-temperature (−77 and −196 °C) studies of **2** in neat films or in ionic (KBr) matrixes showed that under those conditions the compound photoisomerizes to 2-cyanophenol **3** and 2-isocyanophenol **4**. Upon heating to 0 °C, **4** undergoes

thermal cyclization to benzoxazole **1** (Scheme 1).[8, 10] Our previous study on the photochemistry of monomeric benzisoxazole **2** isolated in cryogenic Ar matrixes[5] revealed the isomeric spiro-2*H*-azirine and ketenimine (see below) as key intermediates in the isomerization to 2-cyanophenol **3**. No signs of **4** or **1** were spectroscopically detected. Supported by studies on the chemistry of simple isoxazoles,[13-14] it was postulated that the photochemical mechanism of matrix-isolated benzisoxazoles is initiated by the N−O bond cleavage and formation of a vinylnitrene intermediate.[5, 15] This fascinating nitrene species, having a monovalent nitrogen atom and a triplet ground state,[16-17] was proposed to dictate the subsequent chemistry and explains the observation of different photoproducts found in the low-temperature matrixes.

In contrast to benzisoxazole, the photochemistry of benzoxazole has been much less explored. In polar solvents under air-saturated conditions, UV-excitation of **1** was found to result in dehydrodimerization yielding the 2,2'-dibenzoxazole dimer, with yields up to 90 %.[18] However, in the absence of oxygen, this dimer was not formed. Likewise, in non-polar inert solvents, such as methylcyclohexane, UV-excitation of **1** only leads to trace amounts of the 2,2'-dibenzoxazole dimer. However, the studies performed at −40 °C (in methylcyclohexane), seemed to indicate the formation of a different photoproduct, 2-isocyanophenol **4**, which promptly decayed back to **1** upon heating to room temperature.[18] The thermal reaction of benzoxazole under single pulse shock-tube conditions was also studied.[19] Under those conditions, the main isomerization product was 2-cyanophenol **3**, which subsequently decomposed to cyano-cyclopentadiene and CO.

Herein, we report on the photochemistry of benzoxazole **1** isolated in a low-temperature Ar matrix. Aiming to find out whether there is any pathway connecting benzoxazole **1** and benzisoxazole **2**, this study is also extended to their isomeric 2-cyanophenol **3** and 2-isocyanophenol **4**. As far as we are aware, the narrowband UV-induced photochemistry of monomeric **1**, **3** and **4** has been never reported hitherto, and is addressed in this work for the first time. The three starting compounds (**1**, **3**, **4**) isolated in solid Ar at 12 K, as well as their photoproducts, were characterized experimentally by IR spectroscopy and computationally with the aid of density functional theory (DFT) calculations.

■ RESULTS AND DISCUSSION

Photochemistry of matrix-isolated benzoxazole induced by irradiation at 270 nm

The IR spectrum of benzoxazole **1**, recorded immediately after isolating monomers of this compound in an Ar matrix at 12 K, is presented in Figure S1a. The spectrum is dominated by the absorptions centered at 1525, 1452, 1239, 1106, 1070, 779, 764 and 748/745 cm^{-1}. Strong bands at approximately the same positions have been previously identified in the vapor phase infrared and Raman spectra of this compound, respectively at 1529, 1454, 1240, 1107, 1074, 778, 764 and 746 cm^{-1} (infrared),[20] and at 1528, 1453, 1237, 1107, 1072, 777, 764 and 748 cm^{-1} (Raman).[20-21] The B3LYP/6-311++G(d,p) computed IR spectrum of **1** is shown in Figure S1b. The most intense infrared modes (with IR intensities above 10 km mol^{-1}) are predicted at 1535, 1451, 1234, 1105, 1062, 781, 750, and 742 cm^{-1}, all of them correlating well with the positions of the dominant bands observed in the Ar matrix experimental spectrum.

Monomers of benzoxazole **1** isolated in solid Ar at 12 K were irradiated with frequency-tunable UV laser light generated in an optical parametric oscillator (OPO). The photochemical studies were initiated by searching the lowest energy (or the longest wavelength) of UV-photons that would induce a photochemical reaction. As a reference, we used the wavelength of the origin of the first electronic transition (0–0 of $S_1 \leftarrow S_0$ transition) observed at 274 nm for the compound in the gas phase.[22-23] As anticipated, when the OPO output was tuned in the $300 > \lambda > 277$ nm range, UV-irradiations of **1** did not lead to any spectral changes. This observation is important for the mechanistic analysis presented below. When the OPO was tuned at $\lambda = 270$ nm, near the origin of the first electronic transition of **1** in the gas phase, the IR bands of matrix-isolated **1** started to decrease, and new bands due to photoproducts appeared in the spectrum, most prominently in the range near 2100 cm^{-1}. The intense IR band centered at 2138 cm^{-1} is likely to be associated with the characteristic antisymmetric stretching vibration of a ketene moiety [ν_{as}(C=C=O)],[24-25] assigned to fulvenone[26] as will be explained later in the paper. As it is shown below, the ketene species responsible for this absorption is not directly formed from **1**, but rather from photodecomposition of 2-isocyanophenol **4**. Under conditions of irradiation at $\lambda = 270$ nm, **4** is produced from **1** and undergoes prompt photodecomposition. Large-scale generation and subsequent capture of 2-isocyanophenol **4** in a low-temperature Ar matrix could only be observed upon UV-excitation of **1** at shorter wavelengths (see discussion below). A similar photochemical behavior was observed for matrix-isolated isoxazole.[13] During irradiations

near its first electronic transition origin, isoxazole underwent decomposition (to ketene $H_2C=C=O$ plus hydrogen cyanide HCN), while irradiations at shorter wavelengths resulted in the ring-opening reaction followed by photoisomerizations involving various H-atom shifts.[13]

Photochemistry of matrix-isolated benzoxazole induced by irradiation at 233 nm

The most significant spectral changes were observed when matrix-isolated **1** was exposed to UV laser light tuned at λ = 233 nm. In fact, ~18 min of irradiation at this wavelength resulted in consumption of half of the initial amount of the compound. Concomitantly, various new bands were observed in the IR spectrum registered after the irradiation. Owing to the good correspondence between the IR spectrum of the emerging photoproduct and that simulated for 2-isocyanophenol, these bands were reliably assigned to **4**, as shown in Figure 1. The **1** $\rightarrow$ **4** photoprocess involves cleavage of the C2−O1 bond in **1** and H-shift from C2 to O1. It should be noted here that **4** may adopt two conformations, differing by the orientation of the OH group (cis or trans) in relation to the isocyano (−N≡C) group. However, we have recently demonstrated that the less stable trans form of **4**, once photogenerated in a cryogenic Ar matrix, quickly relaxes into the most stable cis form by means of H-atom quantum mechanical tunnelling,[27] following the same behaviour previously reported for other 2-substituted phenols isolated in solid Ar.[28-30] Consequently, all the observed bands of **4** are due to the most stable cis conformer.

The **1** $\rightarrow$ **4** isomerization is by far the dominating, nearly quantitative, transformation induced by the irradiation at λ = 233 nm. Therefore, we were able to accumulate a significant amount of **4** in the Ar matrix, which allowed its subsequent detailed spectroscopic characterization. All the 18 vibrations in the 2200–400 cm^{-1} range with predicted IR intensities above 2 km mol^{-1} were identified in the experiment, as we have recently reported elsewhere.[27] The main spectral signatures of matrix-isolated **4** are the bands found at 3584 and 2118 cm^{-1}, ascribed to the ν(OH) and ν(N≡C) stretching modes, respectively (see Figure 1). Previously, only the bands due to these two modes of **4** were detected at 3350 and 2130 cm^{-1}, respectively, after photoproduction of **4** from **1** at −196 °C and −77 °C in a KBr matrix or in a neat film.[10]

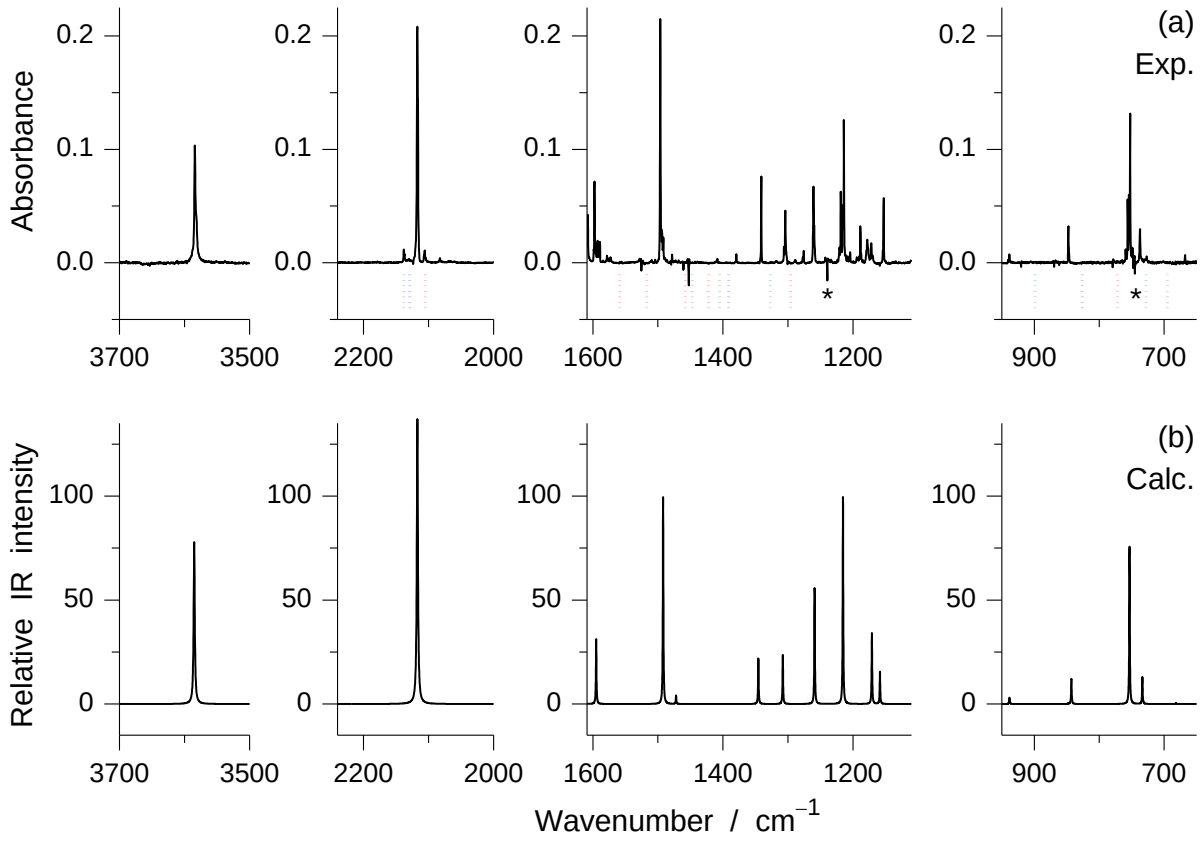

Figure 1. UV-generation of 2-isocyanophenol **4** from benzoxazole **1**: (a) Extracted IR spectrum of the photoproduct generated after irradiation at λ = 233 nm (18 min, ~10 mW) of **1** isolated in an Ar matrix at 12 K. The bands due to the reactant **1** were nullified, only a few negative bands due to **1** (marked with asterisks) remain in the difference spectrum. The dotted lines (below the baseline) show spectral positions of bands due to other photoproducts (**8** - green, **9** - red, **10** - blue) which do not appear at this stage; (b) Simulated IR spectrum of **4**. See experimental section for scaling factors and other details of simulation.

It is worth to comment on the different photochemical behavior of benzoxazole 1 upon irradiation at 233 and 270 nm. Toward this end, we used time-dependent density functional theory (TD-DFT) and computed vertical excitation energies of the low-energy electronic excited states of all relevant species (Table S1). It is known that TD-DFT allows reproduction of the absorption band shapes with good to excellent accuracy.[31] However, many authors point out to systematic overestimation of the TD-DFT computed transition energies, as compared to the experimental results.[32-33] The overestimates reported by different authors range from 0.2 eV,[31] can reach 0.4 eV,[34] and more – about 0.5 eV.[35] With this information in mind, the predicted UV spectra of **1** and **4**, simulated based on the TD-DFT computed data, and presented in Figure S2, qualitatively explain very well the observed photochemistry of **1** and **4**. In fact, we can postulate

that the photoreactivity of **1** is the same at 270 or 233 nm, i.e. formation of isocyanophenol **4**. What changes is that at 270 nm isocyanophenol **4** has a very high absorption (compared to **1**) and **4** quickly decomposes (see discussion below), whereas at 233 nm the absorption of **1** is several times higher than that of **4**, and isocyanophenol **4** is allowed to accumulate.

Photochemistry of matrix-isolated 2-isocyanophenol induced by irradiation at 290 nm

After the *in situ* photoproduction of **4**, subsequent narrowband UV-irradiations were conducted with the objective of inducing transformations in this species. These irradiations were carried out at λ = 290 nm, very close to the wavelength of absorption maximum of **4** measured in ethanol at –77 °C (λ_{max} = 288 nm).[10] It is important to note that **1** does not absorb in UV above 277 nm, as established above, and hence the presence of **1** in the matrix does not interfere with the photochemistry of **4** induced at 290 nm. Irradiations at 290 nm resulted in an appreciable consumption of **4**, accompanied by an increase of the bands due to precursor **1**, demonstrating that under such conditions **4** photoisomerizes back to **1** (see Figure 2).

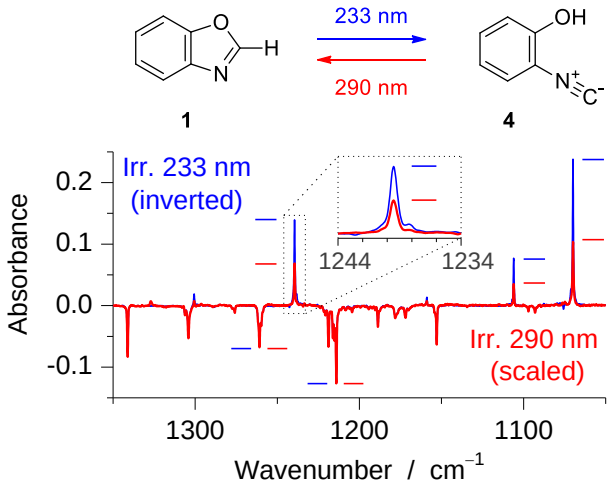

Figure 2. Reversibility of the UV-induced **1** ↔ **4** (benzoxazole ↔ isocyanophenol) photoisomerization. Blue trace: difference IR spectrum (inverted) showing changes upon irradiation at λ = 233 nm (18 min, ~10 mW) of **1** isolated in an Ar matrix at 12 K. Positive bands are due to consumed **1** and negative bands are due to produced **4**. Red trace: difference IR spectrum showing changes after irradiation at λ = 290 nm (6 min, ~30 mW), subsequent to the irradiation at λ = 233 nm. Positive bands are due to photoproducts and negative bands correspond to the consumed species **4**. The intensity of the red trace was scaled (multiplied by 1.5) so that the negative bands in the two difference spectra have the same intensity. The horizontal red and blue bars designate the peak values of the most intense bands (as shown in the inset).

It is likely that the **4** → **1** photoisomerization proceeds through a two-step mechanism, involving initial [1,5] H-atom shift from the hydroxyl to the isocyano group, originating the nitrile-ylide derivative **6**, followed by cyclization of this intermediate to form **1**. The energy profile for the conversion of nitrile-ylide **6** to benzoxazole **1** is presented in Figure 3. It was computed by tracing the corresponding potential energy profile as a function of the distance between the carbon and oxygen atoms (shown in blue in Figure 3).

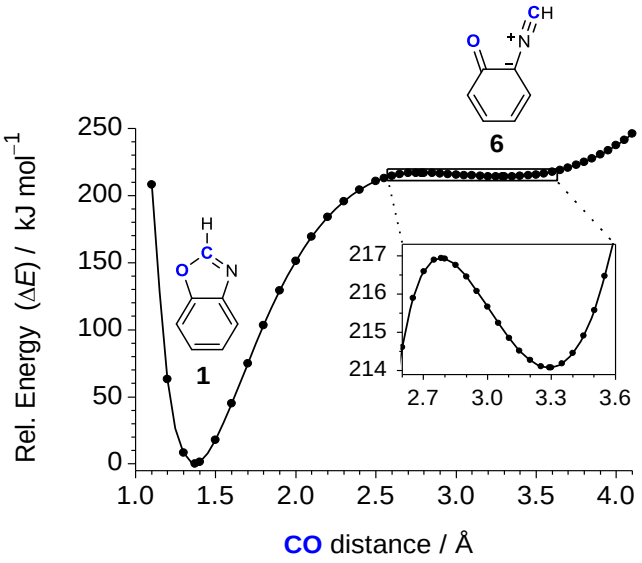

Figure 3. Relaxed potential energy surface (PES) scan connecting open-ring nitrile-ylide **6** (minimum near 3.3 Å) and 1,3-benzoxazole **1** (minimum near 1.4 Å), carried out at the B3LYP/6-311++G(d,p) level of theory as a function of the distance between the carbon and oxygen atoms (highlighted in blue). A fragment of the PES scan between 2.6 and 3.6 Å is expanded in the inset.

As it can be seen in Figure 3, the barrier height for the **6** → **1** conversion in the ground state is very low, amounting to only 3 kJ mol^{-1} at the B3LYP/6-311++G(d,p) level of theory, and can be easily surmounted in an Ar matrix at 15 K. Therefore, as **6** is photoproduced, it should immediately collapse into **1**, impeding its possible detection in the Ar matrix. In a previous study performed in our laboratory,[14] an acetyl nitrile-ylide derivative was identified in an Ar matrix as an intermediate in the photoisomerization of 3,5-dimethylisoxazole to 2,5-dimethyloxazole. Acyclic acetyl nitrile-ylide derivatives have been computed to exhibit two conformers (cis and trans), regarding the mutual orientation of the carbonyl (−C=O) and nitrile-ylide (−C$^-$−N$^+$≡CH) groups with respect to the central C−C bond (see Scheme S1). Only the trans acetyl nitrile-ylide conformer was captured and spectroscopically characterized (the trans → cis conformational

isomerization barrier was estimated to be 54.5 kJ mol^{-1}). The energy barrier of 10 kJ mol^{-1} from the cis acetyl nitrile-ylide to 2,5-dimethyloxazole was found to be not high enough so that cis acetyl nitrile-ylide could be captured.[14] The benzannulated nitrile-ylide **6** (belonging to the present work) can exist *exclusively* as cis isomer, regarding the relative orientation of the carbonyl and nitrile-ylide groups (see Figure 3). It must undergo easy thermal relaxation to **1**, over the low energy barrier in the ground state (3 kJ mol^{-1} only, see inset in Figure 3) even at cryogenic temperatures.

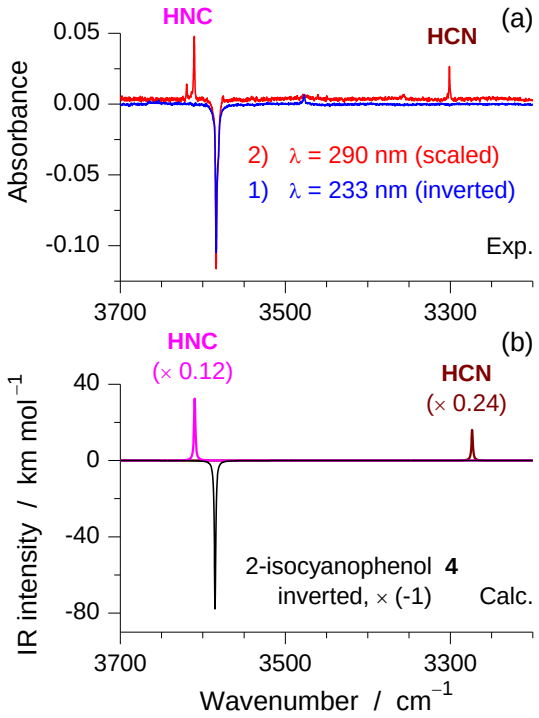

Figure 4. Evidence of a partial photodecomposition of 2-isocyanophenol **4**: (a) Blue and red traces are the same as blue and red traces in Figure 2; (b) Simulated IR spectra. Black: 2-isocyanophenol **4** (intensity multiplied by −1); Pink: **HNC** (intensity multiplied by 0.12); Brown: **HCN** (intensity multiplied by 0.24). The computed B3LYP/6-311++G(d,p) vibrational frequencies in the 3700-3200 cm^{-1} range were scaled by 0.948. See experimental section for other details of the spectral simulation.

The reverse **4** → **1** transformation takes place with only about a half of the yield compared with the forward **1** → **4** photoprocess (Figure 2), i.e. only a half of **4** existing in the matrix converts back to **1**. This suggests that the remaining half of **4** is converted to other photoproducts. These are fulvenone **8** (cyclopenta-2,4-dienylidenemethanone) plus HCN and HNC, resulting from direct decomposition of **4**, and the isomeric species 1-oxo-2-isocyano-2,5-cyclohexadiene **10**, which is a result of a radical recombination process involving

2-isocyanophenoxyl radical **9** as intermediate (see below). The proton stretching modes of matrix-isolated HNC and HCN were identified in this work at 3620/3610 [ν(NH)] and 3301 cm^{-1} [ν(CH)], respectively (Figure 4).[36] These experimental values are in a good match with those reported earlier at 3620 cm^{-1} for ν(NH) of HNC,[37-38] at 3306/3303 cm^{-1} for ν(CH) of HCN,[38-41] as well as with the theoretical wavenumbers computed at 3610 [ν(NH)] and at 3315 cm^{-1} [ν(CH)], for HNC and HCN respectively (see Table 1).

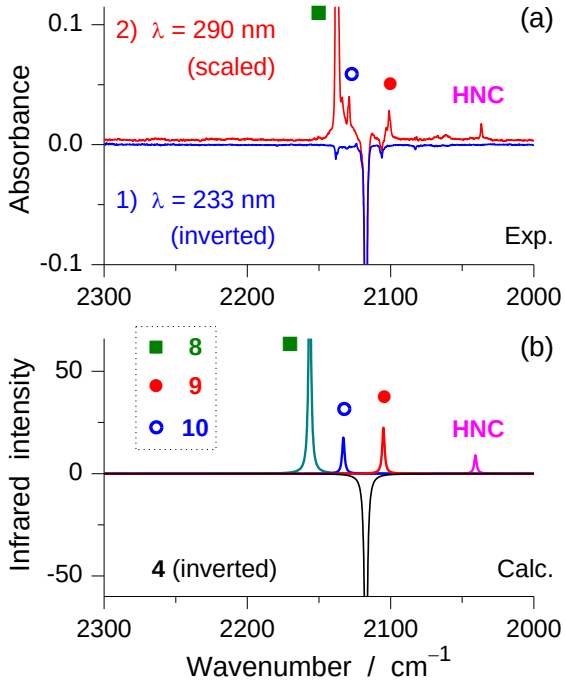

Figure 5. (a) Blue and red traces are the same as blue and red traces in Figure 2; Positive bands are due to **8** (green square), **9** (solid red circle), **10** (open blue circle), and **HNC** (pink) photoproduced from **4**. (b) Simulated spectra. **4** (black, intensity multiplied by −1); **8** (green square, intensity multiplied by 0.08), **9** (solid red circle, intensity multiplied by 0.07), **10** (open blue circle, intensity multiplied by 0.07), **HNC** (pink, intensity multiplied by 0.12). The computed B3LYP/6-311++G(d,p) vibrational frequencies in the 2300-2000 cm^{-1} range were scaled by 0.974. See experimental section for other details of the simulation. The bands due to **4** and **8** are truncated in both frames.

Other bands of HNC and HCN observed in this work also agree with the spectra reported previously for these compounds isolated in Ar matrix.[37-43] The position of the ν(N≡C) band of HNC observed at 2037 cm^{-1} (Figure 5) matches well the computed value of 2041 cm^{-1} (Table 1) and the experimental values 2032 and 2031 cm^{-1} reported previously.[42-43] The δ(HCN) band of hydrogen cyanide was reported earlier[13] to appear at 727/725 cm^{-1}, but in the present experiment it must overlap with an intense IR band of other species (**8**, see Table 1).

Table 1. Experimental and computed infrared absorptions of selected photoproducts generated by irradiation at λ = 290 nm of 2-isocyanophenol **4** isolated in an Ar matrix at 12 K.

Exper.[a]	Computed [b] $\tilde{\nu}$	Computed [b] A^{th}	Sym.	Vibrational assignment [c]
				Benzoxazole (**1**)
1525	1535	51.6	A'	ν(C2=N)
1452	1451	32.7	A'	δ(CH) − ν(CC)
1239	1234	41.1	A'	[ν(C9N) + ν(C8O)] – ν(CC)
1106	1105	21.0	A'	δ(CH) + δ(Bz-ring)
1070	1062	68.8	A'	ν(C2O)
779	781	10.5	A'	ν(CC) + [ν(C9N) + ν(C8O)]
764	750	59.3	A"	τ(Bz-ring) + γ(CH)
748/745	742	33.4	A"	γ(CH) − τ(Bz-ring)
				Fulvenone (or Cyclopenta-2,4-dienylidenemethanone) (**8**)
2138/2133	2156	1398.1	A_1	ν_{as}(C=C=O)
1447	1454	104.7	A_1	ν_s(C=C) + ν_s(C=C=O)
1405 [d]	1407	21.0	A_1	ν_s(C=C) − ν_s(C=C=O)
1327	1331	11.4	A_1	ν_s(C=C=O) − ν(C−C)
1080	1082	11.0	B_2	δ(C3H) − δ(C4H) − δ(C5H) + δ(C6H)
1075	1077	12.8	A_1	δ(C3H) − δ(C4H) + δ(C5H) − δ(C6H)
899 [e]	895	37.5	A_1	ν_s(C−C−C) − δ(ring)
728 / 726 [f]	721	119.5	B_1	γ_a(CH)
576	584	17.6	B_1	τ_a(ring)
				Hydrogen Cyanide (**HCN**)
3301	3315	67.3	Σ	ν(CH)
-	2139	1.9	Σ	ν(C≡N)
728 / 726 [f]	753	84.8	Π	δ(HCN)
				Hydrogen Isocyanide (**HNC**)
3620/3610	3610	271.5	Σ	ν(NH)
2037	2041	74.7	Σ	ν(N≡C)
489/484	486	322.9	Π	δ(HNC)
				2-Isocyanophenoxyl radical (**9**)
2101	2104	321.6	A'	ν(N≡C)
1559	1564	56.1	A'	ν(C2C3) + ν(C5C6) − ν(CO)
1517	1513	20.8	A'	ν(C3C4) − ν(C4C5) − ν(C5C6) − ν(CO) +δ(C4H) − δ(C6H)
1458	1477	18.4	A'	ν(CO) + ν(C2C3)
1422	1408	36.9	A'	ν(C1C2) + ν(C2C3) − ν(C3C4) + ν(C4C5) + δ(C3H) + δ(C5H)
1296	1280	19.9	A'	ν(C2C3) + ν(C4C5) − ν(C5C6) − δ(C3H) − δ(C4H)
1090	1095	19.2	A'	δ_a(ring) − δ(C3H) + δ(C4H) + δ(C5H) − δ(C6H)
772	771	47.0	A"	γ(C3H) + γ(C4H) + γ(C5H) + τ_a(ring)
695	705	28.2	A"	γ(C4H) + γ(C5H) + γ(C6H) + τ_b(ring)
				1-Oxo-2-isocyano-2,5-cyclohexadiene (**10**)
2129	2133	252.9	A'	ν(N≡C)
1696	1712	278.1	A'	ν(C=O)
1405 [d]	1401	22.9	A'	(CH_2) scis
1391	1392	10.3	A'	δ(C5H) + δ(C6H)
1339	1348	19.8	A'	δ(C3H) + ν(C1−C2)
-	1143	17.2	A'	δ(C5H) − δ(C6H)
1100	1109	58.2	A'	ν(C−N) + δ_a(ring) + (CH_2) wag
943	950	23.0	A"	(CH_2) rock − γ(C3H) − γ(C6H)
899 [e]	895	11.2	A'	δ_b(ring)
826	825	24.2	A"	γ(C5H) + γ(C6H) + τ_a(ring)
-	651	15.9	A"	γ(C5H) + γ(C6H) + (CH_2) rock + τ_b(ring)
-	560	10.3	A'	δ(C=O) + δ(C−N)

[a] Bands emerging in the IR spectrum upon 6 min of irradiation of matrix-isolated **4** at λ = 290 nm. [b] Wavenumbers (cm^{-1}) and absolute IR intensities (km mol^{-1}) computed in harmonic approximation at the

B3LYP/6-311++G(d,p) theory level. The computed wavenumbers were scaled by 0.948 [ν(NH)], 0.960 [ν(CH)], 0.974 [ν(N≡C) and ν_{as}(C=C=O)], or 0.983 (all other modes, below 1800 cm^{-1}). [c] Assignment based on animation of vibrations using CHEMCRAFT software (ring atom numbering is given in Scheme 1). For compounds **1**, **8**, **9**, **10** all modes with computed IR intensities over 10 km mol^{-1} are listed. Abbreviations: as = antisymmetric, s = symmetric, ν = stretching, wag = wagging, scis = scissoring, rock = rocking, δ = in-plane bending, γ = out-of-plane bending (four atoms in a trigonal planar arrangement), τ = torsion (four atoms in a sequence), Bz-ring = benzene ring. Signs ''+'' and ''–'' denote vibrations in the same phase and in the opposite phase, respectively. [d,e,f] Assignments of the same experimental bands to overlapping modes of different photoproducts.

In the 3700-3200 cm^{-1} spectral range (Figure 4), the three species (**4**, HNC, HCN) have well-defined non-overlapping bands. From their integrated intensities, weighted by respective computed IR intensities (Table 1), extension of the photodecomposition can be estimated. Considering that about a half of **4** converts back to **1** (Figure 2), the next major photoreaction channel consists in elimination of HNC (12%) plus HCN (24%) making up to about one-third of consumed **4** (Figure 4). The immediate corollary is that the irradiated matrix is likely to contain a detectable photoproduct resulting from decomposition of **4**, with a formula up to C_6H_4O.

The absorption centred at 2138 cm^{-1}, which appears during the irradiation of **1** at λ = 270 nm, also grows in the course of the irradiations at λ = 290 nm (Figure 5), thus confirming that a ketene species responsible for this absorption results indeed from photodecomposition of **4**. Cyclopenta-2,4-dienylidenemethanone **8**, also known as fulvenone[44-45] (Scheme 2) was identified as the product giving rise to this band. Fulvenone **8** has been previously characterized as a major product of the photochemistry of 2-chlorophenol[29] and 2-bromophenol[30] isolated in low-temperature Ar matrices. In those studies, besides a very strong IR band at 2140/2130 cm^{-1} due to the characteristic ν_{as}(C=C=O) ketene mode, other bands were assigned to matrix isolated **8** generated from 2-halophenols (e.g., bands at 1447, 1404, 1327, 896 and 729 cm^{-1}).[29] As shown in Table 1 and Figure 6, bands at nearly the same positions were observed in the IR spectrum recorded after irradiation of matrix-isolated **4** at λ = 290 nm. All nine fundamental modes of **8** with computed IR intensities over 10 km mol^{-1} are nicely reproduced in the present experiment. Additionally, it should be noted that the bands of **8** *do not* appear in the spectrum upon irradiation at λ = 233 nm, as can be seen in Figure 1, the dotted vertical green lines below the baseline. All these data support fulvenone **8** as a product of photodecomposition of **4** at λ = 290 nm (Scheme 2). Consistent with the expectation, fulvenone **8**, formed together with HCN and HNC, has the molecular formula C_6H_4O. The formation of fulvenone **8** from 2-halophenols has been proposed to occur through Wolff-type rearrangement of a singlet ketocarbene **7** (2-oxocyclohexa-3,5-dienylidene) intermediate.[29, 46-48] A similar mechanism is expected for the

4 → **8** photoreaction, as illustrated in Scheme 2. Experimental evidence of ketocarbene **7** was previously obtained by time resolved UV-vis spectroscopy upon photolysis of 2-chlorophenol at λ = 266 nm in hexane and methanol at room temperature, with measured lifetimes of 23 and 5 ps, respectively.[48]

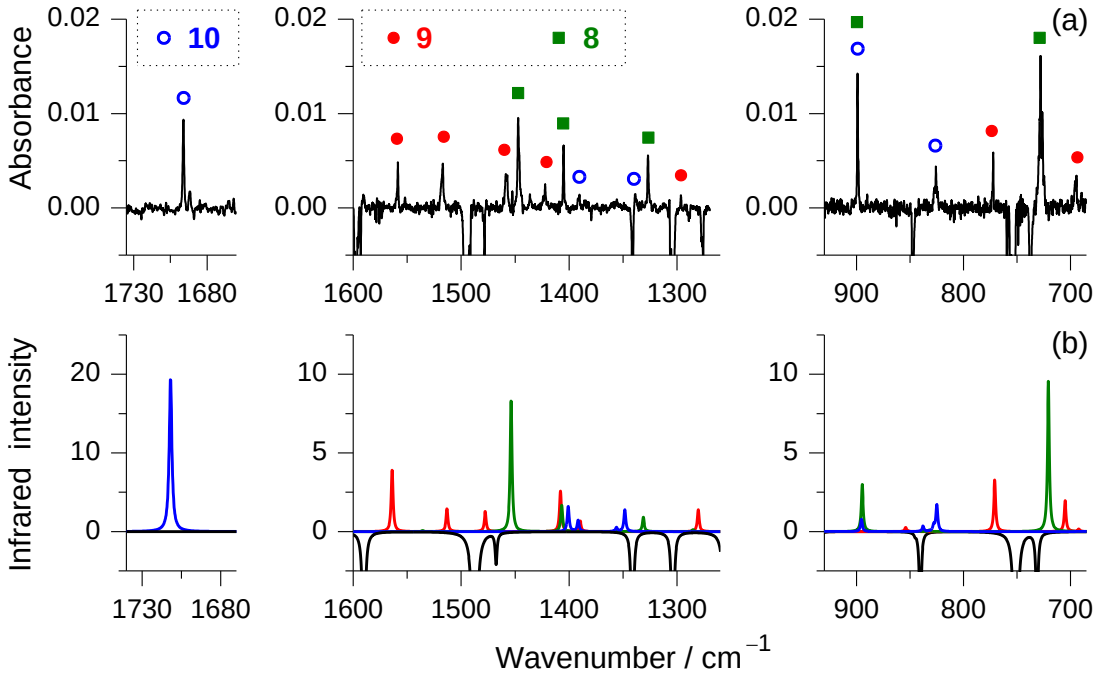

Figure 6. (a) Difference IR spectrum showing the changes after irradiation of **4** at λ = 290 nm (6 min, ~30 mW), subsequent to photogeneration of **4** at λ = 233 nm from **1** (Ar, 12 K). Positive bands are due to photoproducts **8** (green squares), **9** (solid red circles), and **10** (open blue circles). The negative bands (truncated) are due to the consumed reactant **4**. Bands of non-reacting **1** were nullified in the experimental spectrum. (b) Simulated spectra of **4** (black, intensity multiplied by −1), **8** (green, intensity multiplied by 0.08), **9** (red, intensity multiplied by 0.07), and **10** (blue, intensity multiplied by 0.07). The computed B3LYP/6-311++G(d,p) vibrational frequencies below 1800 cm^{-1} were scaled by 0.983. See experimental section for other details of the simulation.

The experimental observation of HNC and HCN resulting from **4**, is the evident proof that 2-isocyanophenol undergoes cleavage of both the single O−H and C(2)−N bonds under λ = 290 nm UV-irradiation. However, as pointed out by Garcia-Garibay and co-authors, C−C (and C−N) bond cleavages do not usually lead to products in crystals unless a second bond cleavage takes place that yields stable products.[49-53] A similar situation can be expected to happen in the case of argon matrices, because radical pairs tend to recombine faster than they can escape,[54] however H is a notorious exception to this rule.[55, 56] Under these conditions, two

possible mechanisms leading to formation of fulvenone **8** can be postulated: (a) concurrent intramolecular H atom shift and C(2)−N bond cleavage, generating HNC and NCH and carbene **7** directly; or (b) initial photocleavage of the OH phenolic bond to produce the hydrogen atom, followed by cleavage of the C(2)−N bond and prompt recombination to yield HCN and HNC and carbene **7**. In both (a) and (b) cases, formation of the transient carbene **7** is followed by its rearrangement to fulvenone **8**. Though both possibilities are compatible with the spectroscopic data and expected chemistry,[49-53] hypothesis (b) seems to be more plausible in view of the experimental detection of the 2-isocyanophenoxyl radical **9**.

The proposed mechanisms are also in agreement with the fact that no band was observed in our experiments that could be ascribed to the CN radical. The vibrational fundamental of the free radical CN isolated in argon matrices has been reported to appear at 2046.0 cm^{-1},[37] as a doublet between 2043 and 2048 cm^{-1},[57] or as a small band at 2050.8 cm^{-1}.[58] No such band was found in our experiments. Moreover, 2-hydroxyphenyl radical **5** (Scheme S2) was previously generated in argon matrices by photolysis ($\lambda > 280$ nm) of 2-iodophenol.[59-60] The strongest infrared bands of **5** were reported at 1448, 1440, 1233, 1163, 820, and 728 cm^{-1}.[59] Even if some of these spectral positions are near absorptions of other photoproducts, some other non-overlapping bands with characteristic frequencies (e.g. 1233 and 820 cm^{-1}) do not appear in our experiments, suggesting that the 2-hydroxyphenyl radical is in fact not formed (see Scheme 2).

The cleavage of only the O−H bond should give rise to 2-isocyanophenoxyl radical **9**, and H-atom. The H atom is invisible in infrared spectra, but 2-isocyanophenoxyl radical **9**, formed by hydrogen detachment from the OH group of **4** (Scheme 2), was unequivocally identified, based on a set of nine bands appearing in the IR spectrum recorded after the performed irradiations (Table 1). The stronger ones were found at 2101 [ν(N≡C)], 1559 [ν(CC)], 1517 [ν(CC) ; δ(CH)] and 772 cm^{-1} [γ(CH)] (Figures 5 and 6). All these nine bands belong to the set of bands with computed IR intensities over 10 km mol^{-1}, and correlate well with the computed wavenumbers of this radical. These bands of **9** *do not* appear in the spectrum upon irradiation at $\lambda = 233$ nm, as demonstrate the dotted vertical red lines below the baseline in Figure 1. It is worth mentioning that the band observed at 1458 cm^{-1} (Figure 6), which is assigned to the ν(CO) mode of **9**, appears at a much higher frequency than the band assigned to the equivalent vibrational mode observed for **4** (1261 cm^{-1}).[27] Such an accentuated shift to higher frequency (+197 cm^{-1}) indicates that the CO bond acquires a considerable double bond character in radical **9**, as

confirmed by the values of the natural bond orders computed for both species at the B3LYP/6-311++G(d,p) level: 1.69 and 1.08, respectively (see Figure S3 for details). These results agree with the structural data previously reported for the change in the order of CO bond within the parent pair, *viz.* phenol and phenoxyl radical.[55, 61-63]

Scheme 2. Reaction pathways in the photochemistry of monomeric 1,3-benzoxazole **1**, 1,2-benzisoxazole **2** (Ref. [5]), 2-cyanophenol **3**, and 2-isocyanophenol **4**, isolated in solid argon at 12-15 K.

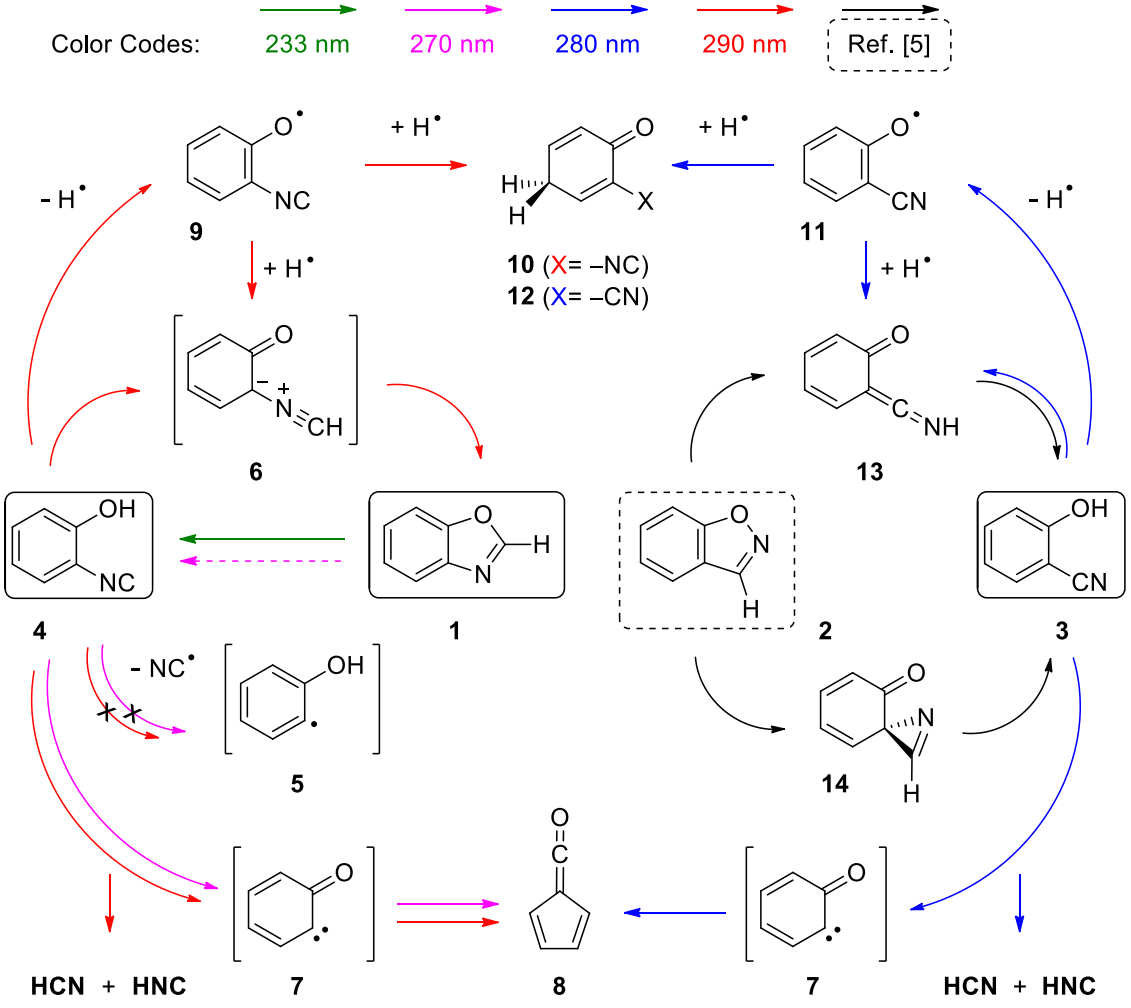

The sharp band emerging at 1696 cm^{-1} in the spectra recorded after the UV-irradiations at λ = 290 nm (Figure 6) is characteristic of the stretching vibration of a non-hydrogen-bonded carbonyl group connected to a six-membered ring.[55, 64] The presence of such a band indicates that an oxo tautomer of **4** should be generated by recombination of the detached hydrogen atom with radical **9**. Among the possible candidates, the one resulting from H-atom recombination at

the *para*-carbon atom (C4, see Figure S3b), with respect to the CO group, 1-oxo-2-isocyano-2,5-cyclohexadiene **10** (Scheme 2), was spectroscopically identified as the photoproduced isomer (see Table 1). The preference of the H-atom to recombine at C4 can be interpreted based on the results of an NBO analysis carried out for the intermediate radical species **9** at the UB3LYP/6-311++G(d,p) level of theory. Among all ring carbon atoms of radical **9**, it is C4 that exhibits a high spin density (0.34), which is nearly equal to the highest value computed for the oxygen atom (0.39) of the same radical (Figure S3a). The data provided by the spin density distribution are also supported by the results of the natural resonance theory (NRT) calculations, which attribute the largest resonance weight to the quinoid structure characterized by a double C=O bond, conjugated with two double C=C bonds (C2=C3 and C5=C6), with the unpaired electron centred at C4 (see Figure S4). This behaviour is in line with that found before for the phenoxyl[61, 63] and 2-cyanophenoxyl[15] radicals. Similarly to **8** and **9**, the bands of **10** *do not* appear among the bands of photoproducts upon irradiation at λ = 233 nm, as can be seen in Figure 1 (dotted vertical blue lines). After comparing the experimental intensities of the bands due to **4**, **9**, and **10** with their computed counterparts, it follows that in the matrix irradiated at λ = 290 nm, each of the photoproducts **9** and **10** is formed in an amount of 7 % (compared to the amount of consumed **4**). Then the overall distribution of photoproducts resulting from **4** (at λ = 290 nm) can be represented as:

4 (100%) $\rightarrow$ **1** (50%) + **HCN** (24%) + **HNC** (12%) + **9** (7%) + **10** (7%).[65-69]

Photochemistry of matrix-isolated 2-cyanophenol induced by irradiation at 280 nm

The photochemistry of matrix-isolated 2-cyanophenol **3** was also investigated by irradiating monomers of the compound trapped in an Ar matrix (15 K) at λ = 280 nm. This wavelength was chosen to directly reproduce the UV-irradiation conditions of **3** with those implemented for UV-irradiation of **2** in the earlier study.[5] Also, this wavelength is not far from the origin of the first electronic transition found for this compound (294 nm) under supersonic jet conditions.[70-71] Two of the reaction pathways identified above for **4** were also observed for **3** (see Scheme 2): one leading to the formation of fulvenone **8**; and the other involving the O–H bond cleavage, yielding in this case 2-cyanophenoxyl radical **11** and the corresponding oxo tautomer **12** (1-oxo-2-cyano-2,5-cyclohexadiene). The identification of these three photoproducts was

based on: (*i*) the good agreement between the computed and experimental IR bands emerging in the spectra recorded after the UV-irradiations (Figure 7 and Table S2); (*ii*) spectral data for analogous products resulting from the photochemistry of **4**; (*iii*) previous IR spectroscopic characterization of **11** in Ar matrix captured upon photolysis of 3-chloro-1,2-benzisoxazole.[15]

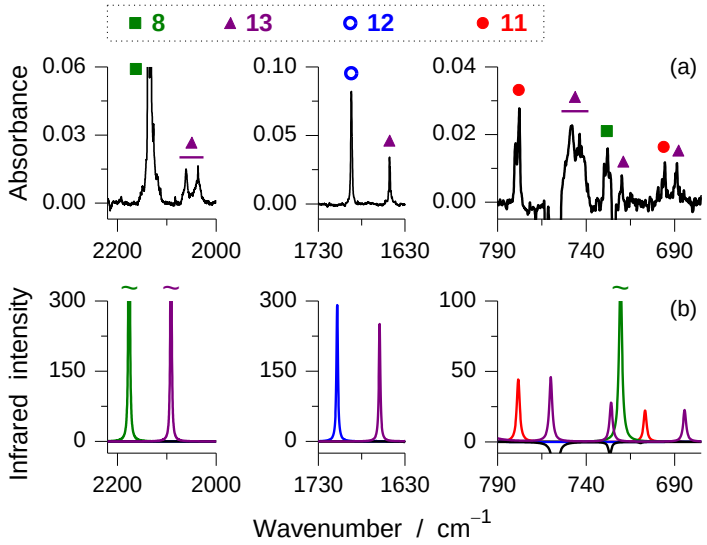

Figure 7. (a) Difference IR spectrum showing the changes after irradiation of 2-cyanophenol **3** at λ = 280 nm (1 min, ~30 mW), in an Ar matrix at 15 K. Positive bands are due to photoproducts **8** (green squares), **11** (solid red circles), **12** (open blue circles), and **13** (triangles). The negative bands (truncated) are due to the consumed reactant **3**. (b) Simulated IR spectra of **3** (black, truncated, intensity multiplied by −1), **8** (green), **11** (red), **12** (blue), and **13** (purple). The computed B3LYP/6-311++G(d,p) wavenumbers below 1800 cm^{-1} were scaled by 0.983, and IR intensities of **8**, **11**, **12**, and **13** were not scaled. See experimental section for other details of the simulation.

A set of additional eight new bands was located at frequencies that cannot be explained by any of the photoproducts identified above. The most prominent ones are centered at 2061/2037, 1648 and 749/744 cm^{-1} (Figure 7). Bands at the same wavenumbers were previously ascribed to ketenimine **13** photogenerated upon irradiation of matrix-isolated benzisoxazole **2** (Ar, 15 K) at λ = 280 nm (Scheme 2).[5] The ketenimine was previously characterized as an intermediate, together with spiro-2*H*-azirine **14**, in the photoisomerization leading to the conversion of benzisoxazole **2** to 2-cyanophenol **3** (Scheme 2).[5] The results obtained in the present study show that **13** is also photogenerated from **3** upon irradiation of this compound at λ = 280 nm, meaning that most probably the two isomers, **3** and **13**, are in photoequilibrium at this wavelength.

■ CONCLUDING DICUSSION

In this work, we undertook combined experimental and computational studies to address the mechanisms of photochemistry induced by narrowband UV-irradiations in the family of isomeric compounds (benzoxazole **1**, benzisoxazole **2**, cyanophenol **3**, and isocyanophenol **4**). Cleavage of the C2−O1 bond and H-shift from C2 to O1 was found to be the dominant photoprocess upon UV-excitation of matrix-isolated **1** at λ = 233 nm, resulting in nearly quantitative generation of 2-isocyanophenol **4**. Subsequent irradiations of the *in situ* produced **4** at λ = 290 nm (where **1** does not absorb) revealed the existence of three reaction pathways: *i*) photodetachment of the H-atom from the OH group of **4**, leading to the generation of 2-isocyanophenoxyl radical **9**, which then recombine at the *para*-carbon atom of the phenyl ring in **9** to yield an oxo tautomer **10**; *ii*) elimination of the CN radical and H-atom (which recombine to give HCN or HNC) and formation of fulvenone **8**, which is most likely a result of a Wolff-type rearrangement of singlet ketocarbene **7**; *iii*) photoisomerization of **4** back to **1**. This last photoprocess is here suggested to proceed through a two-step mechanism involving the formation of nitrile-ylide **6**, which promptly collapses to **1** via a low-energy cyclization barrier in the ground state (predicted to be 3 kJ mol^{-1}). Reaction pathways *i*) and *ii*) also play an important role in the photolysis of 2-cyanophenol **3** (Ar, 15 K) at λ = 280 nm. In addition, **3** was found to photoisomerize to ketenimine **13**, which has been previously proposed as an intermediate in the isomerization of **2** to **3**.[5] Accordingly, an alternative stepwise route for converting **2** into **13** is here proposed, with **14** and **3** acting as intermediates (Scheme 2).

It is worth noticing that under the present experimental conditions, we did not find any crossing point that could permit connection between photochemistries of **1** and **2**. Such a connection would be achieved by means of two reaction pathways: *i*) isocyano ↔ cyano isomerization, leading to the mutual conversion of **3** and **4**, via escape and subsequent recombination of the CN radical resulting in a scrambled CN/NC moiety. Although the cyano → isocyano isomerization has been postulated to occur upon UV-excitation of **3** dissolved in a methanol-water mixture at −77 °C,[10] the results obtained in the present work do not support its occurrence for matrix-isolated **3** or **4**; *ii*) C−C bond cleavage in spiro-2*H*-azirine **14**, originating nitrile-ylide **6**, which, as discussed above (see also Figure 3), immediately collapses to **1**. However, it has been demonstrated that once generated from **2** in a low-temperature Ar matrix, **14** reacts exclusively through the C−N bond cleavage, giving rise to **3**,[5] which has been also reported as being the final product of the photochemistry of **2** in aprotic solvents.[10]

■ EXPERIMENTAL SECTION

Commercial samples of 1,3-benzoxazole **1** (TCI Europe, > 98%) and 2-cyanophenol (also known as 2-hydroxybenzonitrile) **3** (Sigma-Aldrich, 99%) were used as starting compounds for the matrix-isolation experiments. The matrixes were prepared by co-deposition of vapors of **1** and **3** with an excess of the matrix host gas (argon N60, obtained from Air Liquide) onto the CsI optical substrate, cooled down to 15 K. 2-Isocyanophenol **4** was photogenerated *in situ* from **1** isolated in solid Ar at 12 K, as described in ref.[27] The matrix-isolated compounds were then irradiated with narrowband (fwhm < 1 cm^{-1}) UV light from the 290−233 nm range, generated in an optical parametric oscillator pumped with a nanosecond pulsed (pulse frequency 10 Hz) Nd:YAG laser. The progress of the phototransformations was monitored by infrared spectroscopy. Details of the experimental setup, methodology for the preparation of the cryogenic matrixes, laser UV-irradiations and acquisition of IR spectra, can be found elsewhere.[28]

All computations were carried out using the Gaussian 09 software package (Revision D.01).[72] The geometries of all relevant species were fully optimized by employing the DFT(B3LYP) method[73-75] combined with the standard 6-311++G(d,p) basis set.[76-78] Cartesian coordinates of the optimized geometries are provided in Table S3, and the corresponding electronic energies, without and with the zero-point vibrational energy correction, are collected in Table S4. Harmonic vibrational calculations were then performed at the same level of theory on the optimized geometries. With the aim of comparison with the experimental spectra and vibrational assignment, the computed harmonic wavenumbers were scaled. The computed vibrational fundamentals appearing in the 3700-3330 cm^{-1} spectral range [ν(OH) and ν(NH) modes], were scaled by 0.948, as in the preceding work.[27] The computed wavenumbers of ν(CH) modes (appearing in the 3330-2900 cm^{-1} spectral range) were scaled by 0.960, with the scaling factor obtained for this range using data on various monoterpenes that are very abundant with CH groups.[79] The computed vibrational fundamentals appearing in the 2300-2000 cm^{-1} spectral range [ν(N≡C), ν(C≡N), ν_{as}(C=C=O), and ν_{as}(C=C=N) modes], were scaled by 0.974, a factor providing the best match with experiments. Finally, a factor of 0.983 was applied for all modes below 1800 cm^{-1}. It was obtained from least squares linear fit of the experimental vs. B3LYP/6-311++G(d,p) computed harmonic wavenumbers of 2-isocyanophenol (see Ref.[27] for details). The computed scaled wavenumbers and infrared intensities are provided as

Supplementary Information (Table S5). These data were used to simulate IR spectra using the ChemCraft software (version 1.8).[80] The peaks centered at the scaled wavenumbers were convoluted with Lorentzian functions having fwhm = 2 cm^{-1} and peak heights equal to the computed infrared intensities.

A natural bond orbital (NBO) analysis was performed for selected species at the B3LYP/6-311++G(d,p) level using the NBO 6.0 program.[81] Vertical excitation energies of the low-energy electronic excited singlet states (Table S1) were calculated at the B3LYP/6-311++G(d,p) level using the time-dependent density functional theory.[82-83] For the graphical representation, each calculated peak was convoluted with a Lorentzian function having a half-width at half-maximum equal to 0.124 eV (1000 cm^{-1}). The resulting simulated UV spectra of **1** and **4** are presented in Supplementary Information (Figure S2).

■ ACKNOWLEDGMENTS

This work was supported by Project POCI-01-0145-FEDER-028973, funded by FEDER, *via* Portugal 2020 - POCI, and by National Funds *via* the Portuguese Foundation for Science and Technology (FCT). The Coimbra Chemistry Centre (CQC) is supported by the FCT through the projects UIDB/00313/2020 and UIDP/00313/2020, the Chemical Process Engineering and Forest Products Research Centre (CIEPQPF) is supported by the FCT through the projects UIDB/EQU/00102/2020 and UIDP/EQU/00102/2020, also co-funded by FEDER/COMPETE 2020-EU. C.M.N. acknowledges the FCT for an Auxiliary Researcher grant. LaserLab-Coimbra (FCT/ROTEIRO/0152/2013) is also acknowledged. Sandra M. V. Pinto is acknowledged for the participation in preliminary experiments.

■ ASSOCIATED CONTENT

*sı Supporting Information

The Supporting Information is available free of charge at …
Experimental IR spectrum of **1** isolated in an Ar matrix vs. B3LYP/6-311++G(d,p) computed IR spectrum of **1**; Natural bond orders computed for **9** and **4**; Natural spin densities computed for **9**; Predominant resonance structures of **9** resulting from NRT analysis; Simulated UV spectra of **1** and **4** obtained from TD-DFT calculations; Experimental and computed IR spectra of the photoproducts resulting from UV-irradiations of matrix-isolated **3**; Electronic energies, optimized geometries, wavenumbers and IR intensities extracted from the harmonic B3LYP/6-311++G(d,p) vibrational calculations for all relevant species; Wavelengths and oscillator strengths of the low-energy electronic excited singlet states obtained from TD-DFT calculations at the B3LYP/6-311++G(d,p) level.

■ REFERENCES

(1) Oh, Y. J.; Kim, D.; Oh, S.; Jang, E. J.; Won, H. Y.; Jeong, H.; Jeong, M. G.; Choo, H.-Y. P.; Hwang, E. S. Novel benzoxazole derivatives DCPAB and HPAB attenuate Th1 cell-mediated inflammation through T-bet suppression. *Sci. Rep.* **2017,** *7*, 42144.

(2) Youssef, C.; Ammar, H. B.; Belhouchet, M.; Beydoun, K.; Salem, R. B.; Doucet, H.; Dixneuf, P. H. Syntheses of new benzoxazole derivatives. *J. Heterocyc. Chem.* **2011,** *48*, 1126-1131.

(3) Aiello, S.; Wells, G.; Stone, E. L.; Kadri, H.; Bazzi, R.; Bell, D. R.; Stevens, M. F. G.; Matthews, C. S.; Bradshaw, T. D.; Westwell, A. D. Synthesis and Biological Properties of Benzothiazole, Benzoxazole, and Chromen-4-one Analogues of the Potent Antitumor Agent 2-(3,4-Dimethoxyphenyl)-5-fluorobenzothiazole (PMX 610, NSC 721648). *J. Med. Chem.* **2008,** *51*, 5135-5139.

(4) Reiser, A.; Leyshon, L. J.; Saunders, D.; Mijovic, M. V.; Bright, A.; Bogie, J. Fluorescence of aromatic benzoxazole derivatives. *J. Am. Chem. Soc.* **1972,** *94*, 2414-2421.

(5) Nunes, C. M.; Pinto, S. M. V.; Reva, I.; Fausto, R. On the Photochemistry of 1,2-Benzisoxazole: Capture of Elusive Spiro-2*H*-azirine and Ketenimine Intermediates. *Eur. J. Org. Chem.* **2016**, 4152-4158.

(6) Domene, C.; Jenneskens, L. W.; Fowler, P. W. Aromaticity of anthranil and its isomers, 1,2-benzisoxazole and benzoxazole. *Tetrahedron Lett.* **2005,** *46*, 4077-4080.

(7) Ferris, J. P.; Antonucci, F. R. Synthesis of Heterocycles by Photochemical Cyclization of *ortho*-Substituted Benzene Derivatives. *J. Chem. Soc.-Chem. Commun.* **1972**, 126-127.

(8) Ferris, J. P.; Antonucci, F. R.; Trimmer, R. W. Mechanism of the Photoisomerization of Isoxazoles and 2-Cyanophenol to Oxazoles. *J. Am. Chem. Soc.* **1973,** *95*, 919-920.

(9) Ferris, J. P.; Antonucci, F. R. Photochemistry of Ortho-Substituted Benzene Derivatives and Related Heterocycles. *J. Am. Chem. Soc.* **1974,** *96*, 2010-2014.

(10) Ferris, J. P.; Antonucci, F. R. Mechanisms of the Photochemical Rearrangements of Ortho-Substituted Benzene Derivatives and Related Heterocycles. *J. Am. Chem. Soc.* **1974,** *96*, 2014-2019.

(11) Heinzelmann, W.; Märky, M. Photochemistry of Benzisoxazoles. *Helv. Chim. Acta* **1974,** *57*, 376-382.

(12) Lifshitz, A.; Tamburu, C.; Suslensky, A.; Dubnikova, F. Decomposition and isomerization of 1,2-benzisoxazole: Single-pulse shock-tube experiments, quantum chemical and transition-state theory calculations. *J. Phys. Chem. A* **2006,** *110*, 11677-11683.

(13) Nunes, C. M.; Reva, I.; Pinho e Melo, T. M. V. D.; Fausto, R. UV-Laser Photochemistry of Isoxazole Isolated in a Low-Temperature Matrix. *J. Org. Chem.* **2012,** *77*, 8723-8732.

(14) Nunes, C. M.; Reva, I.; Fausto, R. Capture of an Elusive Nitrile Ylide as an Intermediate in Isoxazole-Oxazole Photoisomerization. *J. Org. Chem.* **2013,** *78*, 10657-10665.

(15) Nunes, C. M.; Pinto, S. M. V.; Reva, I.; Rosado, M. T. S.; Fausto, R. Photochemistry of matrix-isolated 3-chloro-1,2-benzisoxazole: Generation and characterization of 2-cyanophenoxyl radical and other reactive intermediates. *J. Mol. Struct.* **2018,** *1172*, 33-41.

(16) Gamage, D. W.; Li, Q.; Ranaweera, R. A. A. U.; Sarkar, S. K.; Weragoda, G. K.; Carr, P. L.; Gudmundsdottir, A. D. Vinylnitrene Formation from 3,5-Diphenyl-isoxazole and 3-Benzoyl-2-phenylazirine. *J. Org. Chem.* **2013,** *78*, 11349-11356.

(17) Sarkar, S. K.; Sawai, A.; Kanahara, K.; Wentrup, C.; Abe, M.; Gudmundsdottir, A. D. Direct Detection of a Triplet Vinylnitrene, 1,4-Naphthoquinone-2-ylnitrene, in Solution and Cryogenic Matrices. *J. Am. Chem. Soc.* **2015,** *137*, 4207-4214.

(18) Grellmann, K. H.; Tauer, E. Symmetric Photodehydrodimerizations Formation of 2,2'-Dibenzoxazole and 2,2'-Dibenzthiazole. *Tetrahedron Lett.* **1974,** *15*, 375-376.

(19) Lifshitz, A.; Tamburu, C.; Suslensky, A.; Dubnikova, F. Thermal reactions of benzoxazole. Single pulse shock tube experiments and quantum chemical calculations. *J. Phys. Chem. A* **2006,** *110*, 4607-4613.

(20) Klots, T. D.; Collier, W. B. Heteroatom Derivatives of Indene. Part 3. Vibrational Spectra of Benzoxazole, Benzofuran, and Indole. *Spectroc. Acta Pt. A-Molec. Biomolec. Spectr.* **1995,** *51*, 1291-1316.

(21) Mille, G.; Davidovics, G.; Chouteau, J. Vibrational Spectra of Benzoxazole (*Sur les spectres de vibration du benzoxazole*). *C. R. Acad. Sci., Ser. B* **1972,** *274*, 532-535.

(22) Gordon, R. D.; Yang, R. F. Vapor Absorption Spectra of Benzoxazole, Benzimidazole, and Benzothiazole near 2850 Å. *Can. J. Chem.* **1970,** *48*, 1722-1729.

(23) Di Lonardo, G.; Trombetti, A.; Zauli, C. Vapour Spectrum of Benzoxazole in the Near Ultraviolet. *J. Chem. Soc. B-Phys. Org.* **1968**, 756-759.

(24) Tidwell, T. T., Chapter 2. Spectroscopy and Physical Properties of Ketenes. In *Ketenes II*, 2 ed.; John Wiley & Sons, Inc.: Hoboken, New Jersey, USA, 2006; pp 27-53.

(25) Breda, S.; Lapinski, L.; Reva, I.; Fausto, R. 4,6-Dimethyl-α-pyrone: a matrix isolation study of the photochemical generation of conjugated ketene, Dewar valence isomer and 1,3-dimethyl-cyclobutadiene. *J. Photochem. Photobiol. A* **2004,** *162*, 139-151.

(26) Koch, R.; Blanch, R. J.; Wentrup, C. Ketene-Ketene Interconversion. 6-Carbonylcyclohexa-2,4-dienone – Hepta-1,2,4,6-tetraene-1,7-dione – 6-Oxocyclohexa-2,4-dienylidene and Wolff Rearrangement to Fulven-6-one. *J. Org. Chem.* **2014,** *79*, 6978-6986.

(27) Lopes Jesus, A. J.; Reva, I.; Nunes, C. M.; Roque, J. P. L.; Pinto, S. M. V.; Fausto, R. Kinetically unstable 2-isocyanophenol isolated in cryogenic matrices: Vibrational excitation, conformational changes and spontaneous tunneling. *Chem. Phys. Lett.* **2020,** *747*, 137069.

(28) Lopes Jesus, A. J.; Nunes, C. M.; Reva, I.; Pinto, S. M. V.; Fausto, R. Effects of Entangled IR Radiation and Tunneling on the Conformational Interconversion of 2-Cyanophenol. *J. Phys. Chem. A* **2019,** *123*, 4396-4405.

(29) Akai, N.; Kudoh, S.; Takayanagi, M.; Nakata, M. Photoreaction mechanisms of 2-chlorophenol and its multiple chloro-substituted derivatives studied by low-temperature matrix-isolation infrared spectroscopy and density-functional-theory calculations. *J. Photochem. Photobiol. A-Chem.* **2001,** *146*, 49-57.

(30) Akai, N.; Kudoh, S.; Takayanagi, M.; Nakata, M. Photoreaction mechanisms of 2-bromophenols studied by low-temperature matrix-isolation infrared spectroscopy and density-functional-theory calculation. *Chem. Phys. Lett.* **2002,** *363*, 591-597.

(31) Jacquemin, D.; Adamo, C., Computational Molecular Electronic Spectroscopy with TD-DFT. In *Density-Functional Methods for Excited States*, Ferré, N.; Filatov, M.; Huix-Rotllant, M., Eds. Springer International Publishing AG: Cham, 2015; Vol. 368, pp 347-375.

(32) Zhou, P. W. Why the lowest electronic excitations of rhodamines are overestimated by time-dependent density functional theory. *Int. J. Quantum Chem.* **2018,** *118*, e25780.

(33) Shao, Y. H.; Mei, Y.; Sundholm, D.; Kaila, V. R. I. Benchmarking the Performance of Time-Dependent Density Functional Theory Methods on Biochromophores. *J. Chem. Theory Comput.* **2020,** *16*, 587-600.

(34) Furche, F.; Ahlrichs, R. Adiabatic time-dependent density functional methods for excited state properties. *J. Chem. Phys.* **2002,** *117*, 7433-7447.

(35) Sobolewski, A. L.; Domcke, W. *Ab initio* potential-energy functions for excited state intramolecular proton transfer: a comparative study of *o*-hydroxybenzaldehyde, salicylic acid and 7-hydroxy-1-indanone. *Phys. Chem. Chem. Phys.* **1999,** *1*, 3065-3072.

(36) Note that HNC or HCN are not produced during irradiation of benzoxazole at 233 nm (blue spectrum in Figure 4a), and appear only during the subsequent irradiation at 290 nm (red spectrum in Figure 4a), at the cost of isocyanophenol.

(37) Milligan, D. E.; Jacox, M. E. Spectroscopic Study of the Vacuum-Ultraviolet Photolysis of Matrix-Isolated HCN and Halogen Cyanides, Infrared Spectra of the Species CN and XNC. *J. Chem. Phys.* **1967,** *47*, 278-285.

(38) Toumi, A.; Piétri, N.; Couturier-Tamburelli, I. Infrared study of matrix-isolated ethyl cyanide: simulation of the photochemistry in the atmosphere of Titan. *Phys. Chem. Chem. Phys.* **2015,** *17*, 30352-30363.

(39) Toumi, A.; Couturier-Tamburelli, I.; Chiavassa, T.; Piétri, N. Photolysis of Astrophysically Relevant Acrylonitrile: A Matrix Experimental Study. *J. Phys. Chem. A* **2014,** *118*, 2453-2462.

(40) King, C. M.; Nixon, E. R. Matrix-Isolation Study of the Hydrogen Cyanide Dimer. *J. Chem. Phys.* **1968,** *48*, 1685-1695.

(41) Satoshi, K.; Takayanagi, M.; Nakata, M. Infrared spectra of $(HCN)_n$ clusters in low-temperature argon matrices. *J. Mol. Struct.* **1997,** *413-414*, 365-369.

(42) Nunes, C. M.; Reva, I.; Rosado, M. T. S.; Fausto, R. The Quest for Carbenic Nitrile Imines: Experimental and Computational Characterization of *C*-Amino Nitrile Imine. *Eur. J. Org. Chem.* **2015**, 7484-7493.

(43) Milligan, D. E.; Jacox, M. E. Infrared Spectroscopic Evidence for the Species HNC. *J. Chem. Phys.* **1963,** *39*, 712-715.

(44) Hemberger, P.; Custodis, V. B. F.; Bodi, A.; Gerber, T.; van Bokhoven, J. A. Understanding the mechanism of catalytic fast pyrolysis by unveiling reactive intermediates in heterogeneous catalysis. *Nat. Commun.* **2017,** *8*, 15946.

(45) Hemberger, P.; Pan, Z. Y.; Bodi, A.; van Bokhoven, J. A.; Ormond, T. K.; Ellison, G. B.; Genossar, N.; Baraban, J. H. The Threshold Photoelectron Spectrum of Fulvenone: A Reactive Ketene Derivative in Lignin Valorization. *ChemPhysChem* **2020,** *21*, 2217-2222.

(46) Bonnichon, F.; Richard, C.; Grabner, G. Formation of an α-ketocarbene by photolysis of aqueous 2-bromophenol. *Chem. Commun.* **2001**, 73-74.

(47) Boule, P.; Richard, C.; David-Oudjehani, K.; Grabner, G. Photochemical behaviour of halophenols in aqueous solution. *Proc. Indian Acad. Sci.-Chem. Sci.* **1997,** *109*, 509-519.

(48) Burdzinski, G.; Kubicki, J.; Sliwa, M.; Réhault, J.; Zhang, Y. L.; Vyas, S.; Luk, H. L.; Hadad, C. M.; Platz, M. S. Mechanistic Aspects of Ketene Formation Deduced from Femtosecond Photolysis of Diazocyclohexadienone, *o*-Phenylene Thioxocarbonate, and 2-Chlorophenol. *J. Org. Chem.* **2013,** *78*, 2026-2032.

(49) Yang, Z.; García-Garibay, M. A. Engineering reactions in crystalline solids: Radical pairs in crystals of dialkyl 1,3-acetonedicarboxylates. *Org. Lett.* **2000,** *2*, 1963-1965.

(50) Yang, Z.; Ng, D.; Garcia-Garibay, M. A. Engineering reactions in crystalline solids: Photochemical generation of secondary and tertiary enol radical pairs from crystalline ketodiesters. *J. Org. Chem.* **2001,** *66*, 4468-4475.

(51) Campos, L. M.; Dang, H.; Ng, D.; Yang, Z.; Martinez, H. L.; Garcia-Garibay, M. A. Engineering reactions in crystalline solids: Predicting photochemical decarbonylation from calculated thermochemical parameters. *J. Org. Chem.* **2002,** *67*, 3749-3754.

(52) Lebedeva, N. V.; Tarasov, V. F.; Resendiz, M. J. E.; Garcia-Garibay, M. A.; White, R. C.; Forbes, M. D. E. The Missing Link Between Molecular Triplets and Spin-Polarized Free Radicals: Room Temperature Triplet States of Nanocrystalline Radical Pairs. *J. Am. Chem. Soc.* **2010,** *132*, 82-84.

(53) Chung, T. S.; Xue, Y.; Carranza, A.; Garcia-Garibay, M. A. Stereospecific photochemistry of Δ^2-1,2,3-triazolines in solution and in the solid state: scope and mechanistic studies. *Photochem. Photobiol. Sci.* **2017,** *16*, 1458-1463.

(54) Pacansky, J.; Bargon, J. Low Temperature Photochemical Studies on Acetyl Benzoyl Peroxide. The Observation of Methyl and Phenyl Radicals by Matrix Isolation Infrared Spectroscopy. *J. Am. Chem. Soc.* **1975,** *97*, 6896-6897.

(55) Giuliano, B. M.; Reva, I.; Lapinski, L.; Fausto, R. Infrared spectra and ultraviolet-tunable laser induced photochemistry of matrix-isolated phenol and phenol-d_5. *J. Chem. Phys.* **2012,** *136*, 024505.

(56) Reva, I.; Nowak, M. J.; Lapinski, L.; Fausto, R. Hydrogen atom transfer reactions in thiophenol: photogeneration of two new thione isomers. *Phys. Chem. Chem. Phys.* **2015,** *17*, 4888-4898.

(57) Jacox, M. E.; Thompson, W. E. Infrared spectra of $ClCN^+$, $ClNC^+$, and $BrCN^+$ trapped in solid neon. *J. Chem. Phys.* **2007,** *126*, 244311.

(58) Borget, F.; Müller, S.; Grote, D.; Theulé, P.; Vinogradoff, V.; Chiavassa, T.; Sander, W. CN radical hydrogenation from solid H_2 reactions, an alternative way of HCN formation in the interstellar medium. *Astron. Astrophys.* **2017,** *598*, A22.

(59) Nagata, M.; Futami, Y.; Akai, N.; Kudoh, S.; Nakata, M. Structure and infrared spectrum of 2-hydroxyphenyl radical. *Chem. Phys. Lett.* **2004,** *392*, 259-264.

(60) Kasai, P. H.; McLeod Jr., D. 2-Hydroxyphenyl and 2-Methoxyphenyl Radicals. Matrix-Isolation Electron Spin Resonance Study. *J. Am. Chem. Soc.* **1974,** *96*, 2338-2342.

(61) Qin, Y.; Wheeler, R. A. Density-functional methods give accurate vibrational frequencies and spin densities for phenoxyl radical. *J. Chem. Phys.* **1995,** *102*, 1689-1698.

(62) Spanget-Larsen, J.; Gil, M.; Gorski, A.; Blake, D. M.; Waluk, J.; Radziszewski, J. G. Vibrations of the phenoxyl radical. *J. Am. Chem. Soc.* **2001,** *123*, 11253-11261.

(63) Cheng, C. W.; Lee, Y. P.; Witek, H. A. Theoretical investigation of molecular properties of the first excited state of the phenoxyl radical. *J. Phys. Chem. A* **2008,** *112*, 2648-2657.

(64) Samanta, A. K.; Pandey, P.; Bandyopadhyay, B.; Chakraborty, T. Keto-enol tautomers of 1,2-cyclohexanedione in solid, liquid, vapour and a cold inert gas matrix: Infrared spectroscopy and quantum chemistry calculation. *J. Mol. Struct.* **2010,** *963*, 234-239.

(65) One of the photoproducts complementary to HCN and HNC is fulvenone **8**. The net production of **8** is about 8% of the reacted **4**, which is less than 36% (the sum of yields of HCN and HNC). This can be explained by the fact that once HCN and HNC are formed, they remain stable in the matrix, because their lowest-energy electronic transitions are situated in the vacuum-UV region of spectrum, below 190 nm (see references 66-68). However, fulvenone **8** can be simultaneously produced and consumed by UV-irradiation at 290 nm, because the electronic absorption spectrum of **8** extends to wavelengths longer than 300 nm (see reference 69 and Table S1). A possible photoproduct of **8** is carbon monoxide, which cannot be identified unequivocally in the experiment because the only infrared absorption of CO appears at exactly the same frequency (2138 cm^{-1}) as the much more intense infrared band of **8**. It is known that fulvenone decomposes thermally to cyclopentadienylidene and CO (see Reference 26).

(66) Herzberg, G.; Innes, K. K. Ultraviolet Absorption Spectra of HCN and DCN. 1. The α-X and β-X Systems. *Can. J. Phys.* **1957,** *35*, 842-879.

(67) Botschwina, P.; Horn, M.; Matuschewski, M.; Schick, E.; Sebald, P. Hydrogen cyanide: Theory and experiment. *Theochem-J. Mol. Struct.* **1997,** *400*, 119-137.

(68) Chenel, A.; Roncero, O.; Aguado, A.; Agúndez, M.; Cernicharo, J. Photodissociation of HCN and HNC isomers in the 7-10 eV energy range. *J. Chem. Phys.* **2016,** *144*, 144306.

(69) Baird, M. S.; Dunkin, I. R.; Hacker, N.; Poliakoff, M.; Turner, J. J. Cyclopentadienylidene. A Matrix Isolation Study Exploiting Photolysis with Unpolarized and Plane-Polarized Light. *J. Am. Chem. Soc.* **1981,** *103*, 5190-5195.

(70) Lahmani, F.; Broquier, M.; Zehnacker-Rentien, A. The *o*-cyanophenol dimer as studied by laser-induced fluorescence and IR fluorescence dip spectroscopy: a study of a symmetrical double hydrogen bond. *Chem. Phys. Lett.* **2002,** *354*, 337-348.

(71) Lahmani, F.; Zehnacker-Rentien, A.; Broquier, M. Electronic and vibrational spectroscopy of jet-cooled complexes of *o*-cyanophenol. *J. Photochem. Photobiol. A-Chem.* **2002,** *154*, 41-52.

(72) Frisch, M. J.; Trucks, G. W.; Schlegel, H. B.; Scuseria, G. E.; Robb, M. A.; Cheeseman, J. R.; Scalmani, G.; Barone, V.; Mennucci, B.; Petersson, G. A., et al. *Gaussian 09*, Revision D.01; Gaussian, Inc.: Wallingford, CT, 2013.

(73) Becke, A. D. Density-functional thermochemistry. III. The role of exact echange. *J. Chem. Phys.* **1993,** *98*, 5648-5652.

(74) Lee, C. T.; Yang, W. T.; Parr, R. G. Development of the Colle-Salvetti correlation-energy formula into a functional of the electron density. *Phys. Rev. B* **1988,** *37*, 785-789.

(75) Vosko, S. H.; Wilk, L.; Nusair, M. Accurate spin-dependent electron liquid correlation energies for local spin density calculations: a critical analysis. *Can. J. Phys.* **1980,** *58*, 1200-1211.

(76) Krishnan, R.; Binkley, J. S.; Seeger, R.; Pople, J. A. Self-consistent molecular orbital methods. XX. A basis set for correlated wave functions. *J. Chem. Phys.* **1980,** *72*, 650-654.

(77) Frisch, M. J.; Pople, J. A.; Binkley, J. S. Self-consistent molecular orbital methods. 25. Supplementary functions for Gaussian basis sets. *J. Chem. Phys.* **1984,** *80*, 3265-3269.

(78) Clark, T.; Chandrasekhar, J.; Spitznagel, G. W.; Schleyer, P. v. R. Efficient Diffuse Function-Augmented Basis Sets for Anion Calculations. 3. The 3-21+G Basis Set for 1st Row Elements, Li-F. *J. Comput. Chem.* **1983,** *4*, 294-301.

(79) Marzec, K. M.; Reva, I.; Fausto, R.; Proniewicz, L. M. Comparative Matrix Isolation Infrared Spectroscopy Study of 1,3- and 1,4-Diene Monoterpenes (α-Phellandrene and γ-Terpinene). *J. Phys. Chem. A* **2011,** *115*, 4342-4353.

(80) Zhurko, G. A. *Chemcraft - Graphical Program for Visualization of Quantum Chemistry Computations*, Version 1.8; http://www.chemcraftprog.com, 2016.

(81) Glendening, E. D.; Badenhoop, J. K.; Reed, A. E.; Carpenter, J. E.; Bohmann, J. A.; Morales, C. M.; Landis, C. R.; Weinhold, F. *NBO 6.0*, Theoretical Chemistry Institute, University of Wisconsin: Madison, WI, 2013.

(82) Bauernschmitt, R.; Ahlrichs, R. Treatment of electronic excitations within the adiabatic approximation of time dependent density functional theory. *Chem. Phys. Lett.* **1996,** *256*, 454-464.

(83) Stratmann, R. E.; Scuseria, G. E.; Frisch, M. J. An efficient implementation of time-dependent density-functional theory for the calculation of excitation energies of large molecules. *J. Chem. Phys.* **1998,** *109*, 8218-8224.

■ GRAPHICAL ABSTRACT

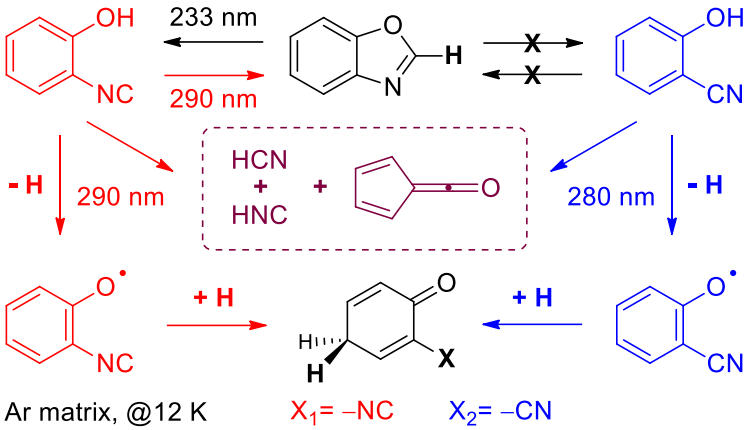

Supporting Information

UV-induced photochemistry of 1,3-benzoxazole, 2-isocyanophenol and 2-cyanophenol isolated in low-temperature Ar matrixes

Igor Reva,*[a,b] A. J. Lopes Jesus,*[c] Cláudio M. Nunes,[a]

José P. L. Roque [a] and R. Fausto [a]

[a] *University of Coimbra, CQC, Department of Chemistry, 3004-535 Coimbra, Portugal.*
[b] *University of Coimbra, CIEPQPF, Department of Chemical Engineering, 3030-790 Coimbra, Portugal*
[c] *University of Coimbra, QC, Faculty of Pharmacy, 3004-295 Coimbra, Portugal.*

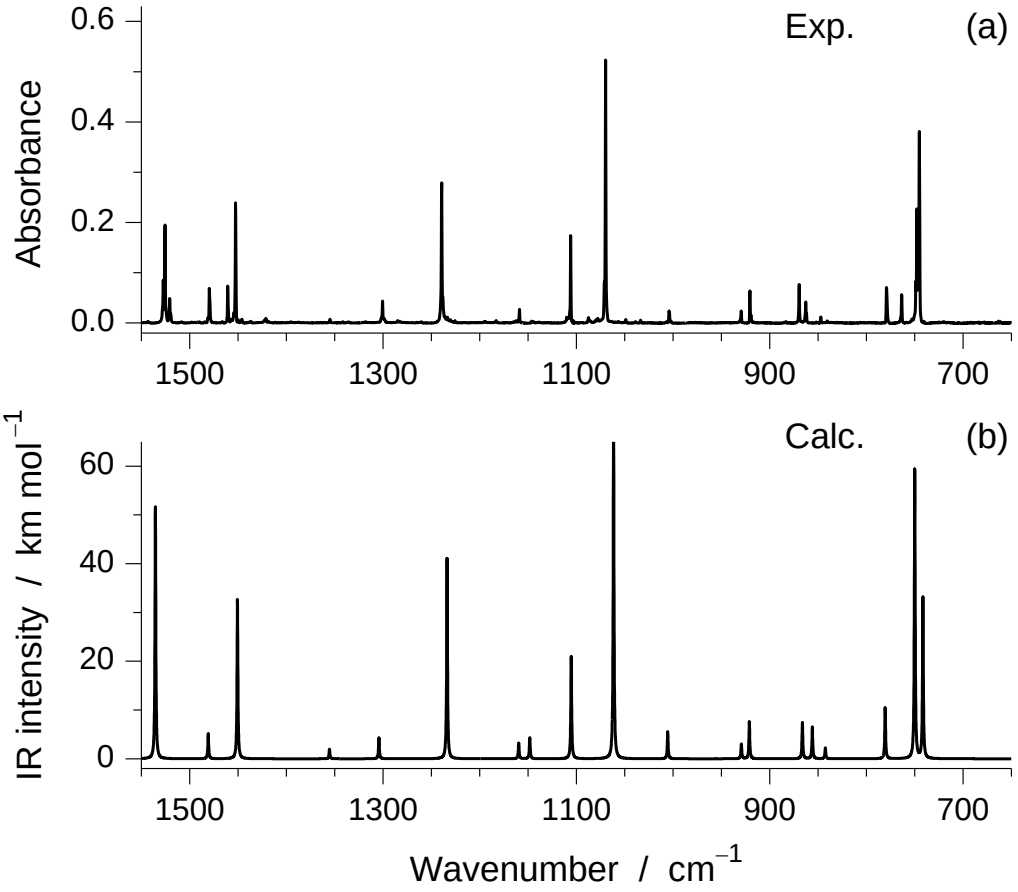

Figure S1. (a) Experimental IR spectrum of benzoxazole **1** isolated in an Ar matrix at 12 K, compared with (b) simulated IR spectrum of **1** based on B3LYP/6-311++G(d,p) harmonic vibrational calculations. The figure shows the most characteristic part of the spectrum, which includes all transitions with computed IR intensities above 10 km mol^{-1}. See the Experimental section for details of the simulation.

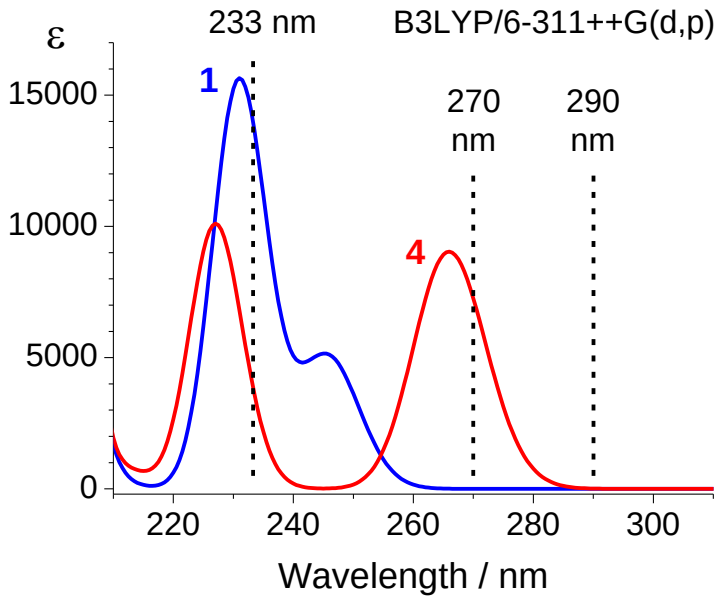

Figure S2. Simulated UV spectra of **1** (blue line) and **4** (red line) obtained from vertical transition energies determined by TD-DFT calculations at the B3LYP/6-311++G(d,p) level (see Table S1). Each calculated transition was convoluted with a Lorentzian function having a half-width at half-height of 0.124 eV (1000 cm^{-1}). Vertical dashed lines correspond to wavelengths of UV-irradiations carried out in this work (233, 270, and 290 nm).

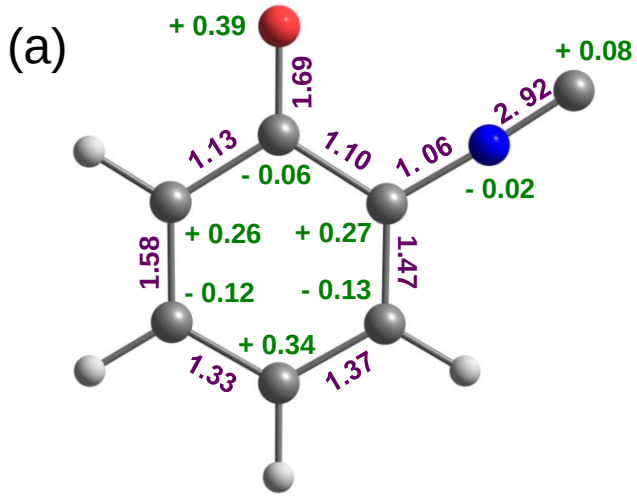

2-isocyanophenoxyl **9**

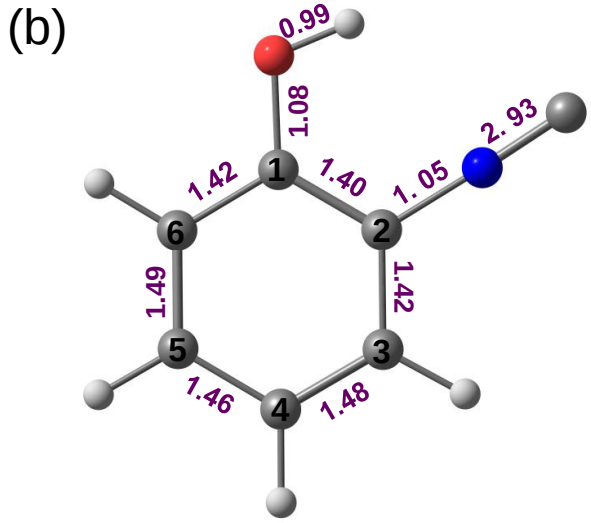

2-isocyanophenol **4**

Figure S3. Natural bond orders (violet) calculated for 2-isocyanophenoxyl radical **9** (a) and 2-isocyanophenol **4** (b), and natural spin densities (green) calculated for **9** (a). Signs "+" and "–" indicate α and β spin, respectively. All values were obtained by means of a Natural Bond Orbital (NBO) analysis carried out at the B3LYP/6-311++G(d,p) level of theory [unrestricted open-shell calculations (UB3LYP) were carried out for the radical].

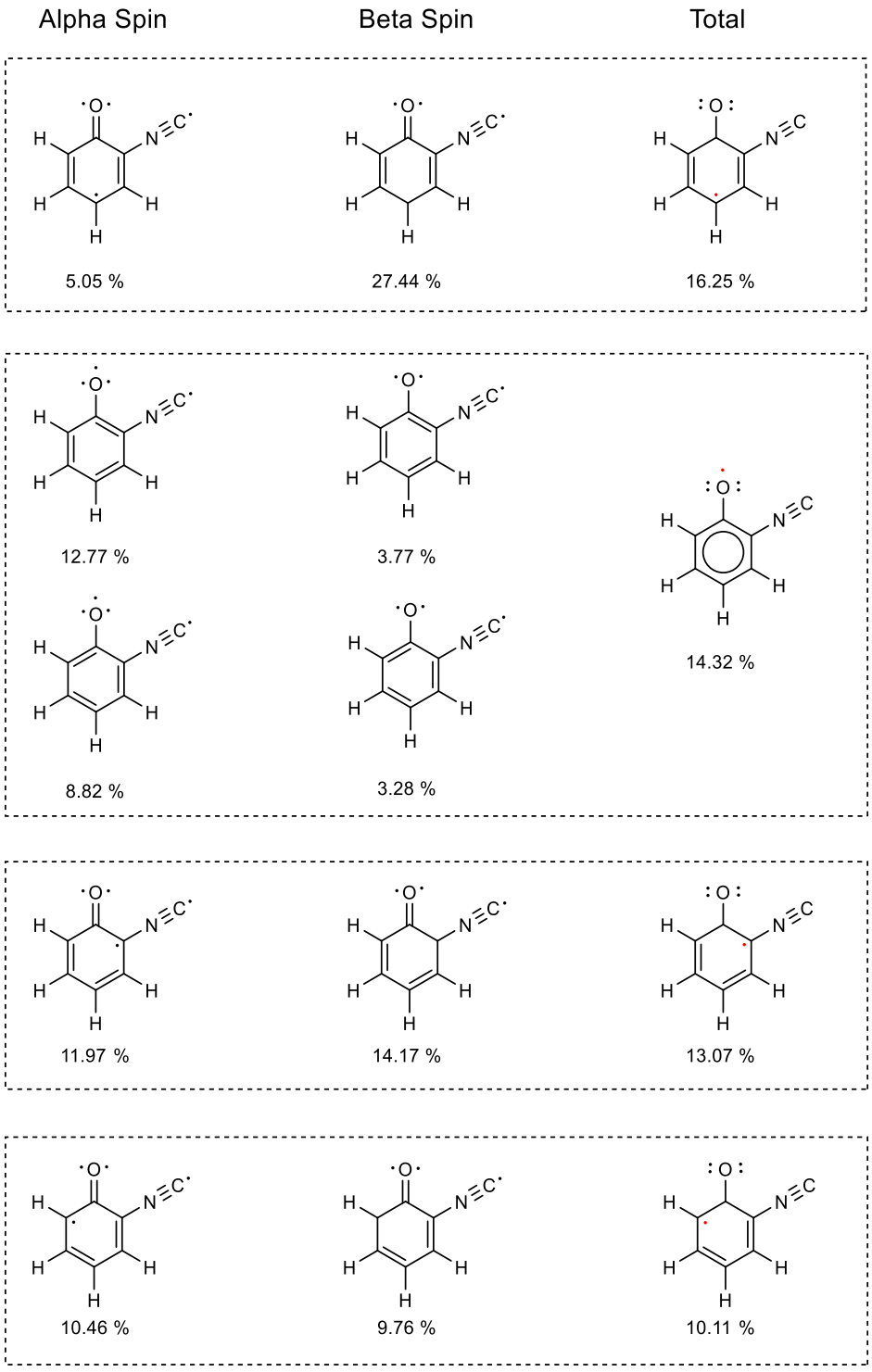

Figure S4. Predominant resonance structures (including the corresponding resonance weights) calculated for 2-isocyanophenoxyl radical **9** by means of a Natural Resonance Theory (NRT) analysis carried out at the UB3LYP/6-311++G(d,p) level of theory.

Scheme S1. Photochemical pathway leading to the generation and capture of the *trans* conformer of the acyclic acetyl nitrile ylide reported in the previous work (Ref. [14]). The corresponding *cis* conformer of the acyclic acetyl nitrile ylide (previous work, Ref. [14]) and the *cis* conformer of the benzannulated nitrile ylide (this work) were not captured.

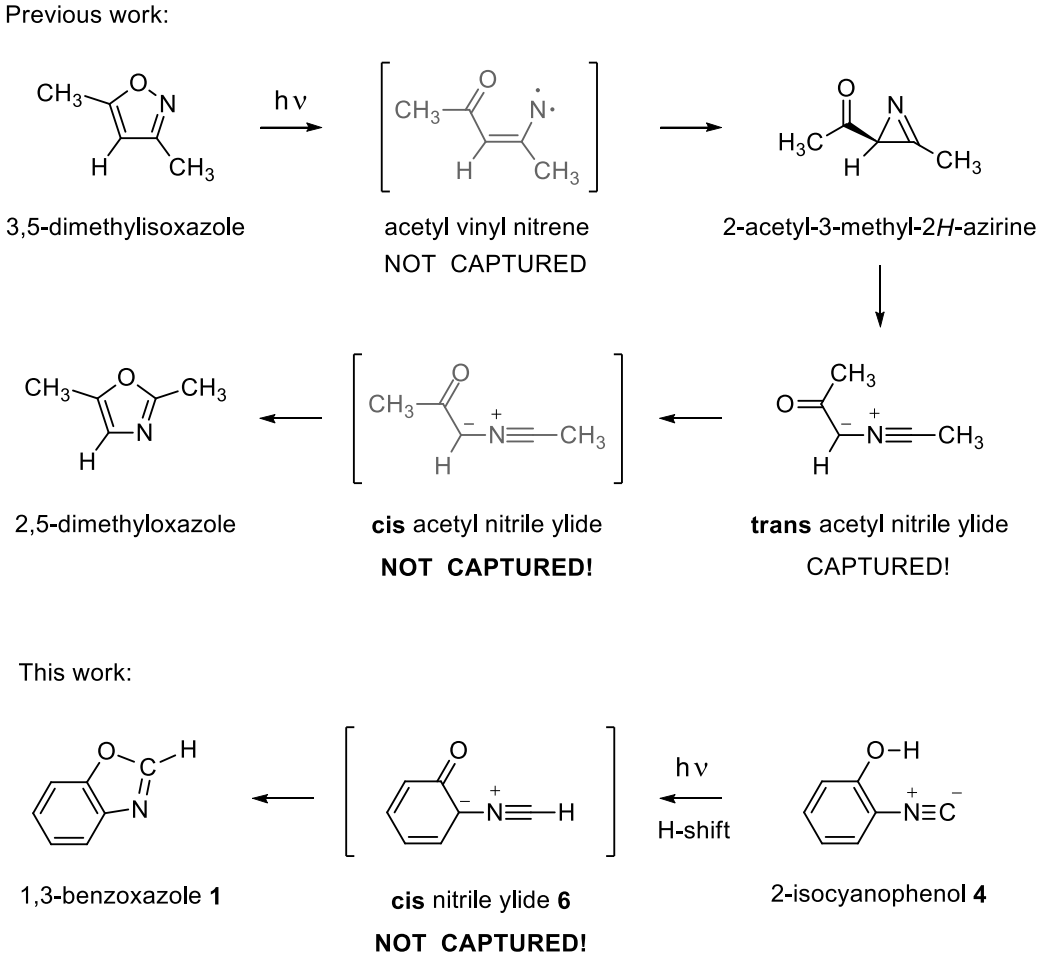

Reference (numbering corresponds to the main text):

(14) Nunes, C. M.; Reva, I.; Fausto, R. Capture of an elusive nitrile ylide as an intermediate in isoxazole-oxazole photoisomerization. *J. Org. Chem.* **2013**, *78*, 10657-10665.

Scheme S2. Photochemical generation of 2-hydroxyphenyl radical **5** from *ortho*-substituted phenols.

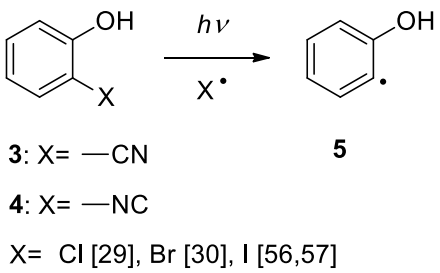

Notes:

In the present work, generation of **5** from either **3** or **4** was not observed.

Nakata and co-authors attempted to photogenerate **5** from three different halophenols as precursors.[29, 30, 56] In the photoreactions of 2-chloro- or 2-bromo-phenols,[29, 30] no infrared spectrum of 2-hydroxyphenyl radical **5** was detectable. A successful generation and detection of **5** previously was achieved by photolysis ($\lambda > 280$ nm) of 2-iodophenol in argon matrices, with characterization by infrared spectroscopy (by Nakata et al.),[56] or by electron spin resonance spectroscopy (by Kasai and McLeod).[57]

References (numbering corresponds to the main text):

(29) Akai, N.; Kudoh, S.; Takayanagi, M.; Nakata, M. Photoreaction mechanisms of 2-chlorophenol and its multiple chloro-substituted derivatives studied by low-temperature matrix-isolation infrared spectroscopy and density-functional-theory calculations. *J. Photochem. Photobiol. A-Chem.* **2001,** *146*, 49-57.

(30) Akai, N.; Kudoh, S.; Takayanagi, M.; Nakata, M. Photoreaction mechanisms of 2-bromophenols studied by low-temperature matrix-isolation infrared spectroscopy and density-functional-theory calculation. *Chem. Phys. Lett.* **2002,** *363*, 591-597.

(56) Nagata, M.; Futami, Y.; Akai, N.; Kudoh, S.; Nakata, M. Structure and infrared spectrum of 2-hydroxyphenyl radical. *Chem. Phys. Lett.* **2004,** *392*, 259-264.

(57) Kasai, P. H.; McLeod Jr., D. 2-Hydroxyphenyl and 2-methoxyphenyl Radicals. Matrix-isolation electron spin resonance study. *J. Am. Chem. Soc.* **1974,** *96*, 2338-2342.

Table S1. Wavelengths (WL / nm) and oscillator strengths (*f*) of the low-energy electronic excited singlet states computed at the B3LYP/6-311++G(d,p) level using the time-dependent density functional theory (TD-DFT) for relevant species within the scope of this work.

Benzoxazole (**1**)			2-Isocyanophenol (**4**)			1-Oxo-2-isocyano-2,5-cyclohexadiene (**10**)		
WL	*f*	Sym.	WL	*f*	Sym.	WL	*f*	Sym.
245.81	0.0459	A'	265.96	0.0831	A'	348.68	0.0000	A"
231.01	0.1435	A'	227.05	0.0929	A'	251.33	0.0000	A"
211.08	0.0011	A"	217.84	0.0002	A"	249.62	0.0606	A'
205.93	0.0083	A"	212.00	0.0062	A"	236.57	0.1037	A'
201.31	0.1853	A'	202.69	0.0003	A"	231.32	0.0032	A"
200.40	0.0017	A"	200.51	0.4193	A'	216.59	0.0562	A'
193.91	0.0004	A"	194.47	0.3869	A'	199.65	0.0012	A"
192.38	0.1329	A'	193.93	0.0029	A"	199.00	0.0012	A'
188.96	0.0037	A"	191.27	0.0023	A"	194.94	0.0145	A"
187.27	0.0053	A"	190.79	0.0013	A"	192.20	0.0001	A"
184.23	0.0075	A"	188.41	0.0199	A"	187.73	0.5395	A'
180.80	0.0030	A"	180.59	0.0011	A"	183.85	0.0028	A"

Benzisoxazole (**2**)			2-Cyanophenol (**3**)			1-Oxo-2-cyano-2,5-cyclohexadiene (**12**)		
WL	*f*	Sym.	WL	*f*	Sym.	WL	*f*	Sym.
257.08	0.0495	A'	269.69	0.0776	A'	354.910	0.0000	A"
234.37	0.1239	A'	226.93	0.0806	A'	262.900	0.0000	A"
207.31	0.0046	A"	210.93	0.0052	A"	245.340	0.0246	A'
204.96	0.0008	A"	206.50	0.0001	A"	241.670	0.1198	A'
198.31	0.2021	A'	199.27	0.5338	A'	217.960	0.0328	A'
197.10	0.0061	A"	198.98	0.0004	A"	215.940	0.0002	A"
194.65	0.1325	A'	191.82	0.2890	A'	200.040	0.0003	A'
191.30	0.0022	A"	190.34	0.0061	A"	192.990	0.3534	A'
185.18	0.0014	A"	188.24	0.0011	A"	188.980	0.0004	A"
184.96	0.0158	A"	187.15	0.0000	A"	188.140	0.0002	A"
183.83	0.3834	A'	184.43	0.0000	A"	186.730	0.0022	A"
178.52	0.0003	A"	178.16	0.0002	A"	182.690	0.0029	A"

Table S1. *Continued*.

Fulvenone (**8**)			Ketenimine (**13**)			Spriro-2*H*-azirine (**14**)		
WL	*f*	Sym.	WL	*f*	Sym.	WL	*f*	Sym.
368.66	0.0001	B_1	396.14	0.0007	A	389.30	0.0002	A
352.96	0.0000	A_2	367.61	0.1269	A	339.99	0.1063	A
295.33	0.0322	B_2	315.78	0.0001	A	287.43	0.0119	A
239.92	0.2455	A_1	263.26	0.0101	A	272.92	0.0018	A
238.30	0.0000	A_2	250.93	0.0171	A	236.20	0.0966	A
216.30	0.0013	B_1	247.59	0.1463	A	221.46	0.0048	A
213.87	0.0000	A_2	231.20	0.0085	A	220.64	0.0034	A
211.73	0.0282	B_1	227.45	0.0169	A	211.75	0.0572	A
194.90	0.0138	B_1	227.24	0.0014	A	209.49	0.0097	A
191.32	0.0000	A_2	218.87	0.0006	A	207.61	0.0023	A
190.21	0.0003	B_1	217.54	0.0051	A	204.27	0.0173	A
189.44	0.0000	A_2	213.37	0.0241	A	199.51	0.0009	A

Table S2. Selected modes in the experimental and calculated IR spectra of the photoproducts generated in an Ar matrix at 15 K, upon UV-excitation of 2-cyanophenol **3** at λ = 280 nm.

Ar, 15 K [a]	Calculated [b]		Sym.	Approximate assignment [c]
	$\tilde{\nu}$	A^{th}		
Fulvenone (or Cyclopenta-2,4-dienylidenemethanone) (**8**)				
2138/2133	2156	1398.1	A_1	ν_{as}(C=C=O)
1447	1454	104.7	A_1	ν_s(C=C) + ν_s(C=C=O)
1405	1407	21.0	A_1	ν_s(C=C) − ν_s(C=C=O)
1327	1331	11.4	A_1	ν_s(C=C=O) − ν(C−C)
1076	1082	11.0	B_2	δ_a(CH)
1071	1077	12.8	A_1	δ_b(CH)
899	895	37.5	A_1	ν_s(C−C−C) − δ(ring)
728	720	119.5	B_1	γ_a(CH)
2-Cyanophenoxyl radical (**11**)				
1558/1550	1560	43.6	A'	ν(C2C3) + ν(C5C6)
1512	1508	11.4	A'	ν(C4C5) − ν(C6C1) ; δ_a(CH)
1459	1468	14.9	A'	ν(CO)
1423	1411	16.3	A'	ν(C1C2) + ν(C4C5) ; δ_b(CH)
1387/1383	1384	10.1	A'	ν(C3C4) + ν(C5C6) ; δ_c(CH)
1291	1284	12.9	A'	ν(C2C3) + ν(C4C5)
1246	1247	6.9	A'	ν(C7C2) + ν(C6C1) ; δ_d(CH)
1088	1087	9.8	A'	δ_a(ring)
780/778	778	44.5	A"	γ_a(CH) ; γ(CO)
699/696	707	22.4	A"	γ_b(CH) ; γ(C−CN)
1-Oxo-2-cyano-2,5-cyclohexadiene (**12**)				
1692	1708	292.8	A'	ν(C=O)
1399 ov.	1398	25.0	A'	(CH_2) scis
1399 ov.	1393	17.3	A'	ν_a(CC) ; δ_a(CH)
1369	1352	26.7	A'	ν_b(CC); δ_b(CH)
1242	1234	17.9	A'	δ_c(CH); ν_c(CC)
1103	1101	36.1	A'	ν_d(CC); δ_a(ring)
951	958	19.4	A"	τ_a(ring) ; γ_a(CH)
902	895	11.0	A'	δ_b(ring) ; ν_e(CC)
827	827	23.6	A"	τ_b(ring); γ(C=O) ; γ_b(CH)
Ketenimine (**13**)				
3363/3356	3347	105.7	A'	ν(NH)
2061/2037	2072	1009.1	A'	ν(C=C=N)$_{as}$
1648	1659	252.8	A'	ν(C=O) − ν_{as}(C=C)
1605/1599	1613	117.8	A'	ν_{as}(C=C) + ν(C=O)
1528/1525	1530	166.6	A'	ν_s(C=C)
1391	1391	12.5	A'	δ_a(CH)
749/744	760	45.7	A"	γ_a(CH); γ(C=O)
639	635	80.7	A"	τ(NH)

[a] Bands observed in the IR spectrum emerging upon 1 min of irradiations at λ = 280 nm. Other bands of the photoproducts could not be unequivocally identified, either due to their low intensity or due to their overlap with bands of other species (designated as "ov"). [b] Scaled wavenumbers (cm^{-1}) and absolute infrared intensities (A^{th}, km mol^{-1}) extracted from the B3LYP/6-311++G(d,p) harmonic vibrational calculations. All modes with computed infrared intensities above 10 km mol^{-1} are included. [c] Abbreviations: ν = stretching, δ = in-plane bending, γ = out-of-plane bending (four atoms in a trigonal planar arrangement), τ = torsion (four atoms in a sequence), s = symmetric, as = antisymmetric, scis = scissoring. [c] Based on animation of vibrations using the CHEMCRAFT software. See G.A. Zhurko, *Chemcraft* - Version 1.8. http://www.chemcraftprog.com, 2016.

Table S3. Cartesian coordinates (Å) of the B3LYP/6-311++G(d,p) optimized geometries of all relevant species within the scope of the present work. Note that all the optimized geometries presented here correspond to the true minima on the respective potential energy surfaces, as confirmed by their vibrational analyses (zero imaginary frequencies, see Table S4).

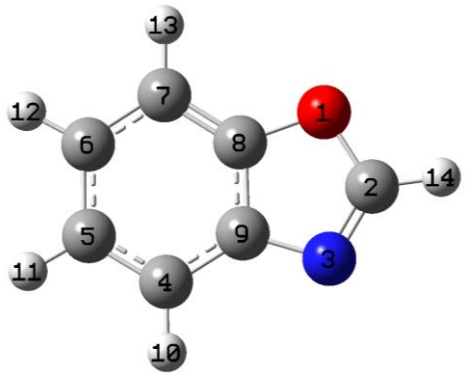

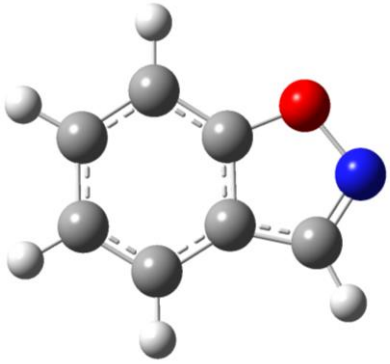

Benzoxazole (**1**), C_s

Electronic energy = -399.82769515 Hartree

C	0.000000	0.718915	0.000000
C	-0.517839	-0.579919	0.000000
C	0.345712	-1.675649	0.000000
C	1.711870	-1.409667	0.000000
C	2.207059	-0.093622	0.000000
C	1.354138	1.009463	0.000000
N	-1.915130	-0.501341	0.000000
O	-1.064715	1.587467	0.000000
H	-0.039965	-2.687542	0.000000
H	2.414731	-2.234597	0.000000
H	3.278657	0.067938	0.000000
H	1.725068	2.026322	0.000000
C	-2.157139	0.761248	0.000000
H	-3.117671	1.252917	0.000000

Benzisoxazole (**2**), C_s

Electronic energy = -399.78587583 Hartree

O	-1.010383	1.608320	0.000000
C	0.345919	-1.692568	0.000000
C	1.709406	-1.442275	0.000000
C	2.209091	-0.123419	0.000000
C	1.366273	0.980211	0.000000
C	0.000000	0.708386	0.000000
C	-0.520019	-0.589793	0.000000
H	-0.036218	-2.706507	0.000000
H	2.408141	-2.270373	0.000000
H	3.281847	0.032211	0.000000
H	1.742539	1.994937	0.000000
N	-2.231291	0.902085	0.000000
C	-1.935912	-0.365001	0.000000
H	-2.742755	-1.084668	0.000000

Table S3. *Continued*

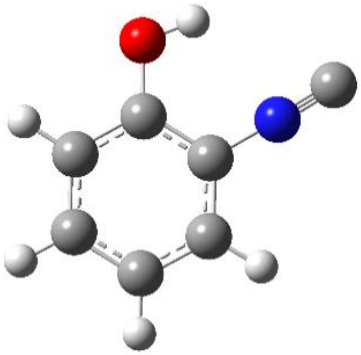

2-Isocyanophenol (**4**), C_s

Electronic energy = -399.79188096 Hartree

C	-0.689459	-0.591012	0.000000
C	0.000000	0.634723	0.000000
C	1.397734	0.668763	0.000000
C	2.115315	-0.518875	0.000000
C	1.432742	-1.738598	0.000000
C	0.044067	-1.777758	0.000000
N	-0.743886	1.804162	0.000000
C	-1.402749	2.777604	0.000000
O	-2.042383	-0.665998	0.000000
H	-2.426889	0.220601	0.000000
H	1.896175	1.629993	0.000000
H	3.197807	-0.495589	0.000000
H	1.989007	-2.668700	0.000000
H	-0.495743	-2.716534	0.000000

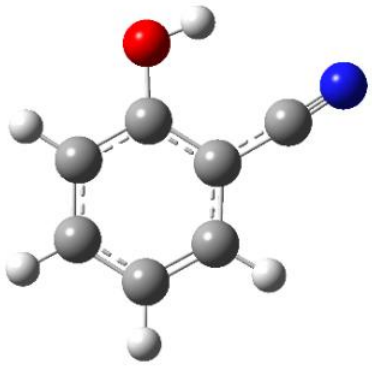

2-Cyanophenol (**3**), C_s

Electronic energy = -399.82770616 Hartree

C	-0.655536	-0.623266	0.000000
C	0.000000	0.625257	0.000000
C	1.404173	0.680280	0.000000
C	2.147425	-0.488684	0.000000
C	1.489185	-1.723469	0.000000
C	0.103106	-1.795237	0.000000
C	-2.004375	-0.743878	0.000000
N	-2.427493	0.125706	0.000000
O	-0.793689	1.809393	0.000000
H	-1.496541	2.728989	0.000000
H	1.889719	1.648311	0.000000
H	3.229220	-0.444142	0.000000
H	2.066097	-2.641204	0.000000
H	-0.414746	-2.746213	0.000000

Table S3. *Continued*

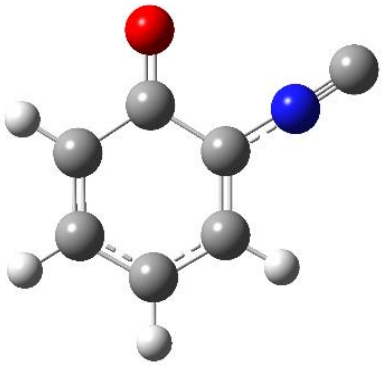

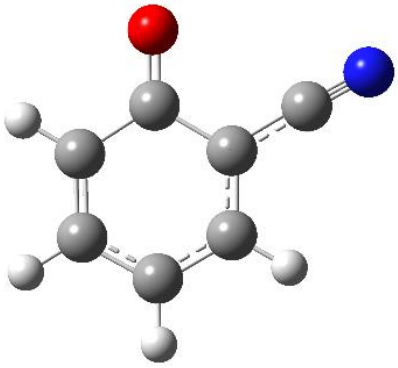

2-Isocyanophenoxyl radical (**9**), C_s [a]

Electronic energy = -399.14253446 Hartree

C	-0.832415	-0.551394	0.000000
C	0.000000	0.664954	0.000000
C	1.382768	0.585669	0.000000
C	2.010760	-0.663919	0.000000
C	1.257316	-1.858483	0.000000
C	-0.112927	-1.813519	0.000000
N	-0.631997	1.877676	0.000000
C	-1.224303	2.895247	0.000000
O	-2.072097	-0.494726	0.000000
H	1.967253	1.497477	0.000000
H	3.093203	-0.711612	0.000000
H	1.772733	-2.812029	0.000000
H	-0.719623	-2.711088	0.000000

2-Cyanophenoxyl radical (**11**), C_s [a]

Electronic energy = -399.17607957 Hartree

C	-0.826513	-0.578691	0.000000
C	0.000000	0.638691	0.000000
C	1.383508	0.548847	0.000000
C	2.012333	-0.703473	0.000000
C	1.256935	-1.894421	0.000000
C	-0.114648	-1.845225	0.000000
C	-0.645261	1.906532	0.000000
N	-1.138875	2.952144	0.000000
O	-2.068104	-0.526106	0.000000
H	1.979200	1.453711	0.000000
H	3.094697	-0.752807	0.000000
H	1.769201	-2.849799	0.000000
H	-0.724260	-2.740824	0.000000

[a] unrestricted open-shell optimization.

Table S3. *Continued*

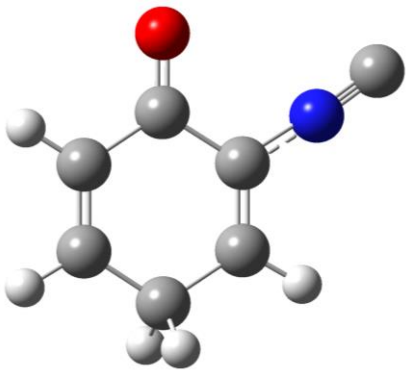

1-Oxo-2-isocyano-2,5-cyclohexadiene (**10**), C_s

Electronic energy = -399.75878128 Hartree

C	0.897006	-0.509088	0.000000
C	0.000000	0.693889	0.000000
C	-1.339838	0.585216	0.000000
C	-2.035733	-0.732176	0.000000
C	-1.129055	-1.918413	0.000000
C	0.205333	-1.811970	0.000000
N	0.619882	1.925176	0.000000
C	1.220916	2.934520	0.000000
O	2.108606	-0.407628	0.000000
H	-1.947755	1.483750	0.000000
H	-2.712477	-0.785748	0.866336
H	-1.599075	-2.897330	0.000000
H	0.851988	-2.682003	0.000000
H	-2.712477	-0.785748	-0.866336

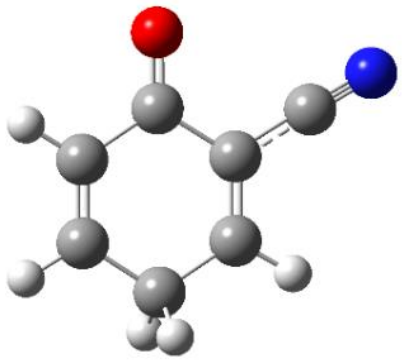

1-Oxo-2-cyano-2,5-cyclohexadiene (**12**), C_s

Electronic energy = -399.79304944 Hartree

C	0.901801	-0.533197	0.000000
C	0.000000	0.665079	0.000000
C	-1.341429	0.536866	0.000000
C	-2.026079	-0.785881	0.000000
C	-1.108236	-1.964081	0.000000
C	0.224838	-1.844139	0.000000
O	2.113599	-0.423001	0.000000
H	-1.966772	1.424053	0.000000
H	-2.703386	-0.840324	0.865915
C	0.611664	1.959193	0.000000
N	1.082630	3.013234	0.000000
H	0.880065	-2.707727	0.000000
H	-2.703386	-0.840324	-0.865915
H	-1.569079	-2.947349	0.000000

Table S3. *Continued*

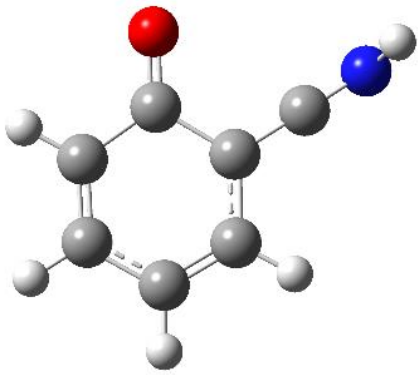

Ketenimine (**13**), C_1

Electronic energy = -399.78044062 Hartree

C	-1.548045	1.073716	-0.022326
C	-0.088246	1.043306	0.005113
C	0.489205	-0.340097	0.008671
C	-0.355522	-1.513024	0.024446
C	-1.703682	-1.373988	0.011818
C	-2.293805	-0.060768	-0.014162
H	-2.003214	2.056958	-0.039410
H	0.107515	-2.492926	0.036438
H	-2.344795	-2.246685	0.016040
H	-3.376666	0.015090	-0.027305
C	1.824793	-0.442001	0.004755
O	0.611559	2.052440	0.029823
N	3.013807	-0.510236	-0.137801
H	3.679847	-0.503178	0.630368

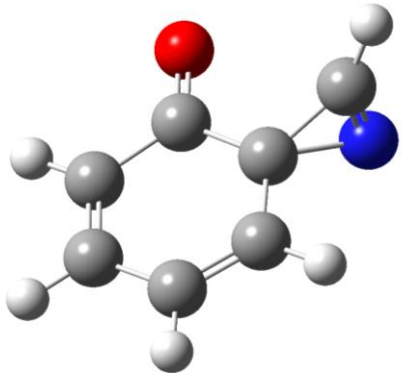

Spiro-2*H*-azirine (**14**), C_1

Electronic energy = -399.73262436 Hartree

C	-1.323008	1.196473	-0.038954
C	0.130560	1.025415	0.013852
C	0.614422	-0.401079	0.052927
C	-0.354523	-1.495542	0.058384
C	-1.677353	-1.235499	0.036421
C	-2.157938	0.131344	-0.018039
H	-1.690243	2.214486	-0.093416
H	0.023921	-2.511919	0.069731
H	-2.397867	-2.044562	0.042344
H	-3.230924	0.292652	-0.052605
C	2.010939	-0.607660	0.487936
H	2.699735	-0.645220	1.321906
O	0.917727	1.961947	0.047374
N	1.970711	-0.668820	-0.746020

Table S3. *Continued*

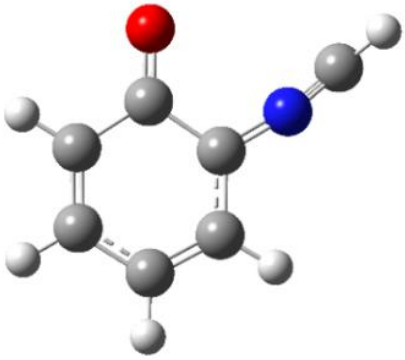

Nitrile-ylide (**6**), C_1

Electronic energy = -399.74615672 Hartree

C	-1.437476	1.153322	-0.010741
C	0.011762	1.013423	0.005954
C	0.466236	-0.402736	0.013611
C	-0.436846	-1.506935	0.013174
C	-1.779410	-1.273131	0.004594
C	-2.268763	0.074284	-0.007224
H	-1.820286	2.166978	-0.021306
H	-0.035393	-2.513923	0.017709
H	-2.479616	-2.098908	0.003821
H	-3.342650	0.232313	-0.015246
O	0.803183	1.958496	0.013762
N	1.774012	-0.580942	0.012803
C	2.942832	-0.535373	-0.127433
H	3.844385	-0.524964	0.463694

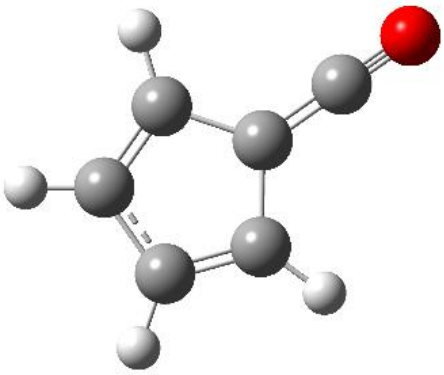

Fulvenone (**8**), C_{2v}. Extended name: Cyclopenta-2,4-dienylidenemethanone

Electronic energy = -306.29592608 Hartree

C	0.000000	0.000000	1.647108
C	0.000000	1.180068	-0.540429
C	0.000000	0.723624	-1.826768
C	0.000000	-0.723624	-1.826768
C	0.000000	-1.180068	-0.540429
C	0.000000	0.000000	0.320045
O	0.000000	0.000000	2.801050
H	0.000000	1.347325	-2.709900
H	0.000000	-1.347325	-2.709900
H	0.000000	-2.201444	-0.192570
H	0.000000	2.201444	-0.192570

Table S4. Electronic energies of all relevant species computed at the B3LYP/6-311++G(d,p) level. [a]

Structure [b]	E_{el} E_h	ΔE_{el} kJ mol^{-1}	E_{el} + ZPE E_h	$\Delta(E_{el}$ + ZPE) kJ mol^{-1}
[7C, 5H, N, O]				
1	-399.827695	0.03	-399.722456	5.63
2	-399.785876	109.83	-399.681358	113.53
3 *	-399.827706	0.00	-399.724601	0.00
4	-399.791881	94.06	-399.689588	91.93
6	-399.746157	214.11	-399.646163	205.94
10	-399.758781	180.96	-399.657740	175.54
12	-399.793049	90.99	-399.691335	87.34
13	-399.780441	124.10	-399.679203	119.19
14	-399.732624	249.64	-399.631985	243.16
[7C, 4H, N, O]$^{\bullet}$				
9	-399.142534	88.07	-399.053567	86.28
11 *	-399.176080	0.00	-399.086430	0.00
[6C, 5H, O]$^{\bullet}$				
5	-306.869348		-306.778180	
[6C, 4H, O]				
^{1}**7**	-306.171340	327.10	-306.089863	332.44
^{3}**7**	-306.223762	189.47	-306.145759	185.68
8 *	-306.295926	0.00	-306.216481	0.00
[C, H, N]				
HCN *	-93.454504	0.00	-93.438145	0.00
HNC	-93.431553	60.26	-93.415853	58.53
NC$^{\bullet}$	-92.738850		-92.733960	
H$^{\bullet}$	-0.502257		-0.502257	

[a] E_{el} – electronic energy; ZPE – zero-point vibrational energy; $E_h \approx 2625.5$ kJ mol^{-1};
[b] Asterisks (*) designate structures with the lowest relative energy in a given set of isomers with the same composition, which is specified in brackets; bullets (•) designate radicals (doublet manifold, unrestricted B3LYP calculations); ^{1}**7** and ^{3}**7** superscripts indicate the closed shell singlet and triplet manifolds, respectively.

Table S5. Wavenumbers ($\tilde{\nu}$ / cm^{-1}) and IR intensities (A^{th} / km mol^{-1}) extracted from harmonic B3LYP/6-311++G(d,p) vibrational calculations carried out for relevant species within the scope of the present work. [a]

Benzoxazole (**1**)		Benzisoxazole (**2**)		2-Cyanophenol (**3**)		2-Isocyanophenol (**4**)	
$\tilde{\nu}$	A^{th}	$\tilde{\nu}$	A^{th}	$\tilde{\nu}$	A^{th}	$\tilde{\nu}$	A^{th}
3131.75	0.50	3099.49	1.20	3572.43	85.92	3585.15	78.05
3077.08	3.40	3079.15	2.50	3077.08	3.87	3078.03	3.26
3072.80	7.32	3067.52	12.02	3072.31	4.16	3072.35	3.59
3059.35	8.87	3056.00	7.14	3062.28	3.20	3063.96	5.01
3046.08	2.17	3046.07	0.80	3049.33	2.54	3050.57	2.04
1626.26	6.25	1622.64	23.68	2254.79	64.72	2117.26	137.51
1609.05	3.91	1607.38	1.94	1624.75	43.33	1620.23	19.34
1535.48	51.64	1526.12	24.00	1584.63	38.81	1594.96	31.46
1480.83	5.17	1478.78	2.65	1487.08	80.99	1492.02	99.48
1450.60	32.72	1433.04	13.72	1468.20	32.84	1472.11	3.94
1355.43	1.97	1359.74	10.16	1344.01	27.52	1345.50	21.94
1304.24	4.38	1307.85	2.91	1311.26	19.83	1307.97	23.75
1281.01	0.01	1256.70	6.23	1253.13	40.51	1259.02	56.02
1233.79	41.11	1231.10	15.71	1221.39	109.07	1215.40	99.52
1159.63	3.23	1179.91	16.63	1176.72	42.07	1170.90	33.96
1148.22	4.34	1149.65	5.04	1159.46	24.73	1158.50	15.56
1105.28	20.99	1118.95	9.11	1096.85	1.54	1094.61	3.00
1061.52	68.77	1009.79	6.37	1033.20	11.56	1032.23	12.95
1005.55	5.60	962.45	0.02	974.09	0.10	965.27	0.07
956.12	0.005	935.74	1.83	946.47	2.09	938.23	3.13
929.35	3.04	935.47	7.65	856.07	0.67	847.81	0.33
921.08	7.62	882.50	9.62	843.16	10.88	842.88	12.10
866.21	7.42	868.96	15.99	757.43	67.87	753.36	76.20
855.91	6.54	858.78	35.75	726.58	9.02	733.56	13.16
842.46	2.23	842.21	3.25	709.36	0.80	681.90	0.45
780.58	10.53	767.21	7.03	602.22	0.29	578.39	1.43
749.97	59.34	747.23	73.73	571.58	2.58	550.43	0.57
741.54	33.37	718.22	0.19	558.37	5.25	547.38	2.25
623.22	0.85	619.48	3.01	495.97	10.69	464.95	1.12
618.52	3.70	604.15	10.06	465.62	0.10	440.06	0.17
566.78	0.002	554.69	0.65	413.32	109.29	398.50	112.66
538.68	1.14	532.05	1.14	392.16	3.96	359.34	6.54
418.46	7.19	420.47	3.18	382.94	3.97	355.91	1.02
415.35	4.01	396.19	3.63	230.22	0.02	229.08	0.04
253.95	0.72	248.86	2.55	138.58	7.17	140.52	4.91
218.64	3.56	205.99	0.18	129.20	2.68	134.00	2.10

Table S4. *Continued*

Nitrile-ylide (**6**)		Fulvenone (**8**)		2-Isocyanophenoxyl radical (**9**)		1-Oxo-2-isocyano-2,5-cyclohexadiene (**10**)	
$\tilde{\nu}$	A^{th}	$\tilde{\nu}$	A^{th}	$\tilde{\nu}$	A^{th}	$\tilde{\nu}$	A^{th}
3144.90	92.10	3115.68	1.86	3075.31	2.59	3063.01	4.12
3071.22	9.76	3111.99	3.24	3070.98	2.51	3048.37	3.09
3064.30	9.17	3089.99	3.18	3061.03	4.43	3031.87	7.33
3049.05	1.29	3078.00	3.35	3049.22	1.95	2875.25	2.28
3033.14	12.76	2156.40	1398.09	2105.03	321.58	2868.89	4.90
2040.06	613.93	1535.64	0.77	1563.92	56.09	2132.98	252.88
1646.68	249.91	1453.71	104.67	1513.11	20.78	1711.91	278.10
1596.26	106.71	1406.91	20.99	1477.69	18.40	1666.00	1.54
1516.05	166.90	1331.32	11.45	1408.02	36.85	1629.21	6.06
1456.75	24.46	1285.17	1.55	1389.72	9.57	1400.84	22.86
1391.41	12.03	1186.36	0.02	1280.44	19.88	1391.71	10.28
1286.81	32.17	1081.90	11.03	1246.49	2.69	1356.17	3.61
1266.13	1.79	1077.39	12.85	1159.65	0.98	1348.43	19.79
1186.10	12.02	1015.33	1.11	1140.19	7.14	1230.13	7.50
1149.42	14.76	899.04	0.00	1095.44	19.16	1186.20	0.09
1113.81	5.75	894.63	37.50	1007.50	0.91	1142.54	17.20
987.29	5.42	871.78	0.00	968.66	0.41	1109.44	58.19
978.40	0.07	831.86	1.26	944.03	5.16	1023.74	8.31
936.31	0.61	720.58	119.55	857.59	0.04	1001.53	1.05
859.68	1.73	680.67	0.00	853.94	3.78	949.83	22.98
840.31	11.70	645.55	8.46	770.75	47.03	895.36	11.21
768.91	38.43	583.88	17.58	704.96	28.23	837.76	4.96
729.12	3.63	561.53	0.00	692.16	2.22	827.83	5.53
697.55	9.44	549.32	0.78	569.08	2.80	824.85	24.24
682.87	50.92	519.47	2.03	549.23	5.16	673.77	9.72
584.39	101.79	152.79	1.31	497.61	1.25	650.90	15.85
568.86	64.69	125.58	0.11	453.33	1.33	559.55	10.29
538.59	62.60			433.83	0.82	536.21	0.55
482.76	299.21			365.71	0.90	442.27	2.00
470.82	536.82			325.70	0.00	422.24	0.81
439.06	25.21			196.98	3.19	366.38	3.62
395.14	8.53			135.48	0.70	322.66	0.71
371.20	20.97			112.45	0.01	300.20	2.93
196.81	1.26					169.59	0.99
112.10	5.13					132.95	0.55
107.01	7.85					90.77	0.03

Table S4. *Continued*

2-Cyanophenoxyl radical (**11**)		1-Oxo-2-cyano-2,5-cyclohexadiene (**12**)		Ketenimine (**13**)		Spriro-2*H*-azirine (**14**)	
$\tilde{\nu}$	A^{th}	$\tilde{\nu}$	A^{th}	$\tilde{\nu}$	A^{th}	$\tilde{\nu}$	A^{th}
3074.98	2.67	3063.39	3.81	3346.56	105.76	3086.32	1.70
3070.09	3.06	3042.15	2.65	3069.66	8.93	3068.00	6.06
3059.33	3.10	3031.90	7.23	3064.11	8.64	3063.42	10.83
3048.96	1.98	2875.97	1.71	3048.09	1.27	3044.91	1.87
2253.84	0.93	2869.36	3.48	3032.60	11.85	3033.54	8.69
1560.26	43.59	2281.50	9.60	2072.38	1009.10	1763.85	24.98
1508.40	11.36	1708.28	292.82	1659.29	252.74	1681.83	274.11
1468.53	14.92	1663.27	0.99	1613.01	117.77	1634.71	30.19
1410.80	16.30	1620.86	0.32	1530.44	166.64	1553.63	51.90
1384.18	10.06	1397.71	24.98	1444.86	3.32	1427.58	3.01
1283.78	12.86	1392.87	17.27	1390.99	12.54	1378.45	15.09
1247.10	6.95	1357.88	2.67	1291.64	21.11	1275.32	17.33
1154.00	3.09	1352.33	26.66	1245.25	2.14	1194.76	43.10
1136.30	1.43	1233.62	17.86	1185.73	19.03	1168.02	42.71
1087.39	9.81	1186.63	0.05	1149.16	15.68	1141.34	56.25
1010.02	1.12	1141.72	11.39	1105.82	15.39	1102.07	11.98
974.51	0.46	1100.50	36.05	988.85	0.08	1022.02	17.00
953.29	4.34	1018.55	5.33	981.02	6.25	997.75	0.09
863.75	0.07	1004.35	1.25	947.11	0.28	969.08	2.63
849.33	2.23	958.39	19.44	854.57	5.34	966.94	2.47
778.34	44.52	895.00	11.02	845.32	16.02	861.59	4.87
706.73	22.42	840.59	5.41	805.44	583.77	849.30	13.67
687.66	0.95	826.73	23.62	759.97	45.74	787.62	17.86
591.13	0.75	822.60	2.71	725.93	27.86	764.05	16.38
551.94	3.56	669.13	8.28	684.40	22.55	745.86	39.98
530.62	9.06	654.20	9.89	635.44	80.71	677.83	3.35
469.32	1.19	585.06	6.53	607.20	14.88	590.32	8.28
456.91	3.99	538.49	0.39	558.62	8.68	541.90	2.58
375.25	0.99	500.81	10.05	518.04	48.32	525.28	5.96
360.10	0.20	444.86	3.12	475.94	9.05	509.16	10.15
200.88	4.22	374.24	4.96	454.07	3.69	406.09	7.97
151.64	1.84	345.71	0.08	378.79	3.41	391.81	1.97
109.11	0.01	303.40	3.99	366.41	9.94	276.79	9.89
		173.68	1.76	190.12	1.77	270.29	4.19
		150.17	1.73	137.73	2.55	207.88	1.68
		84.92	0.00	83.02	4.84	78.82	4.42

[a] Computed wavenumbers are scaled as described in the Experimental section.